2022-06-03

Effect of High Temperature on Physical and Mechanical Properties of Clay Shales (Caprock)

Dovletov, Shamammet

UNIVERSITY OF CALGARY

Effect of High Temperature on Physical and Mechanical Properties of Clay Shales (Caprock)

by

Shamammet Dovletov

A THESIS

SUBMITTED TO THE FACULTY OF GRADUATE STUDIES

IN PARTIAL FULFILMENT OF THE REQUIREMENTS FOR THE

DEGREE OF MASTER OF SCIENCE

GRADUATE PROGRAM IN CIVIL ENGINEERING

CALGARY, ALBERTA

JUNE, 2022

Abstract

The complex structure of heavy crude oil and bitumen requires enhanced oil recovery methods such as cyclic steam stimulation and steam-assisted gravity drainage to recover effectively. These methods are operated at high temperature ranges. Thus, it is crucial to understand the effect of high temperatures on such operations. This thesis aimed to investigate the changes in physical and mechanical properties of clay shale caprock due to pre-heating under high temperatures. For this purpose, intact clay shale cores were recovered from a site near Long Lake in Alberta. To investigate the effect of pre-heating on clay shale's strength and deformation characteristics twelve samples were trimmed and prepared. Samples were pre-heated up to 20, 150, 300 and 600 °C and thereafter cooled down to ambient temperature naturally. The variation of mechanical properties of clay samples due to the pre-heating was examined in triaxial compression tests. Changes in the composition and crystalline structure of the clay samples were determined through X-ray fluorescence and X-ray diffraction analysis. The experimental results indicated clay samples becoming stiffer (with increased Young's modulus and lowered Poisson's ratio) with increasing temperature. Also, the friction angle and cohesive strength of the clay sample increased with temperature. These findings indicate an increasing trend in the mechanical strength of clay samples with temperature. The failure of the clay samples at low confining pressure was mainly due to shear dilation, while compression was the cause of failure at higher confinement pressure.

Acknowledgements

I wish to thank my supervisor Dr. Ron Chik-Kwong Wong, who inspired me in the field of geotechnical engineering research. Since I began working in the Civil Engineering department at the University of Calgary, he has been supportive. Dr. Wong had the initial thesis topic and supported me by showing what it means to be a good teacher. He was not only my supervisor but my mentor and friend. His patience, flexibility, genuine caring and concern, and faith in me during the dissertation process enabled me to complete my MSc program.

I would like to express my special appreciation and thanks to the lab technicians, Mr. Wu and Dr. Bin Xu, who helped me in conducting my experiments. They helped me to understand and analyze the data obtained by experimenting. Their support played a vital role in the completion of my program.

I would also like to thank my family and friends who always supported me and taught me about hard work and self-respect, persistence, and how to be independent. I could never finish this work without your help and support.

Table of Contents

List of figures

List of tables

List of abbreviations

ϕ	angle of friction
G	shear stiffness
C_c	compression index
c'	cohesion
E	Young's modulus
ν	Poisson's ratio
ζ	mass loss rate
m_1, m_2	masses of specimens before and after thermal treatment, respectively
TC	Triaxial Compression Test
q	deviatoric stress
ε_a	axial strain
ε_v	volumetric strain

Chapter 1

1 Introduction

An increase in world population and industrialization of developing countries will heavily affect the global energy demand in a few decades (Sagar et al., 2005). Figure 1.1 bends depict that the global energy consumption will increase substantially and mainly rely on fossil fuels. Also, Figure 1.1 indicates the transition of consumption from coal to oil and gas in the past five decades. Therefore, it is important to examine new prospects to recover hydrocarbons to meet increasing global oil demand. Additionally, Dudley (2018) reported that the estimated oil demand increase will reach 15 MMb/d by 2035.

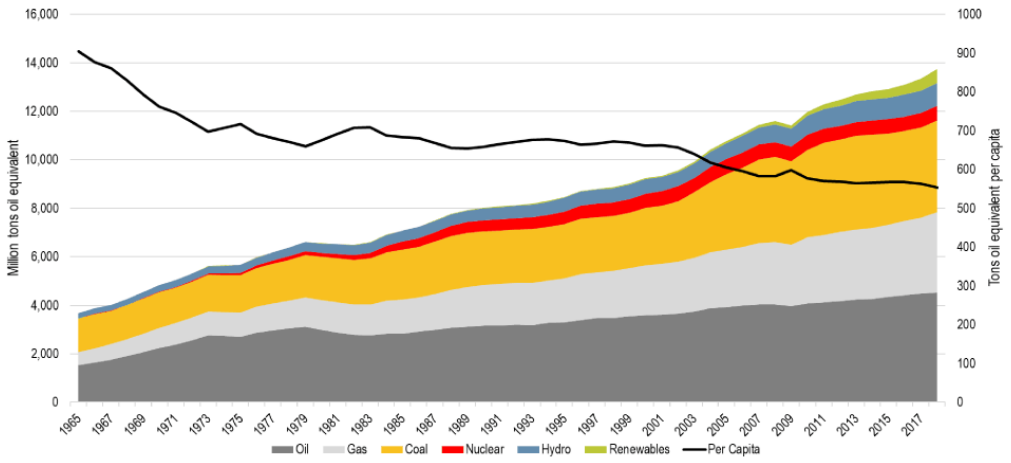

Figure 1.1: Global energy consumption by sector, 1965 – 2018 (Dudley, 2018)

As shown in Figure 1.2, conventional reservoirs comprise only 30% of total reserves. However, unconventional reserves account for 70% of total reserves. The

challenges of unconventional reserves are the necessity of complex technology compared to conventional reserves. Moreover, the continuous depletion of conventional resources makes it vital to explore unconventional reserves such as heavy oil and bitumen (Sims et al., 2007).

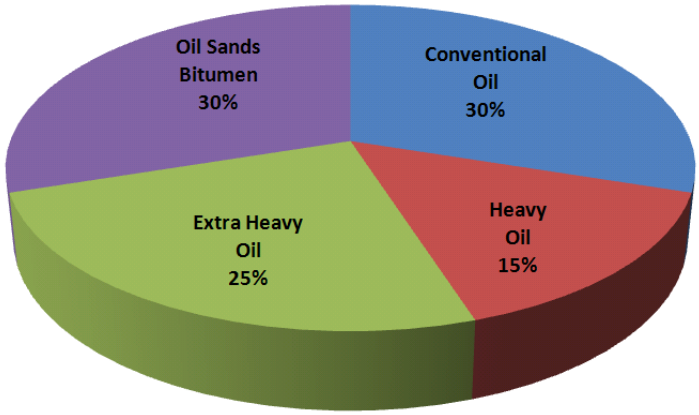

Figure 1.2: Conventional versus unconventional world oil reserves (Golpour & Smith, 2017)

According to Nasr and Ayodele (2005), most of the world's heavy oil and oil sands are deposited in Canada and Venezuela. As shown in Figure 1.3, Alberta has the largest resources of crude bitumen, estimated to hold 2.36 x 10^{11} m^3 (Zhou, 2019). Furthermore, 80% of these reserves could be retrieved using in-situ thermal treatments. However, thermal operations at high temperatures significantly affect clay shales and clay minerals. As the temperature increases further, new cracks form and propagate towards each other, which is associated with the physical and chemical changes of clay after heating (Sims et al., 2007). These physical and chemical changes in the properties of clay shale caprock can substantially influence

the production (Nasr & Ayodele, 2005; Tian et al., 2014). Therefore, it is vital to understand thermal recovery processes and in-situ operations and their effect on unconventional reserves.

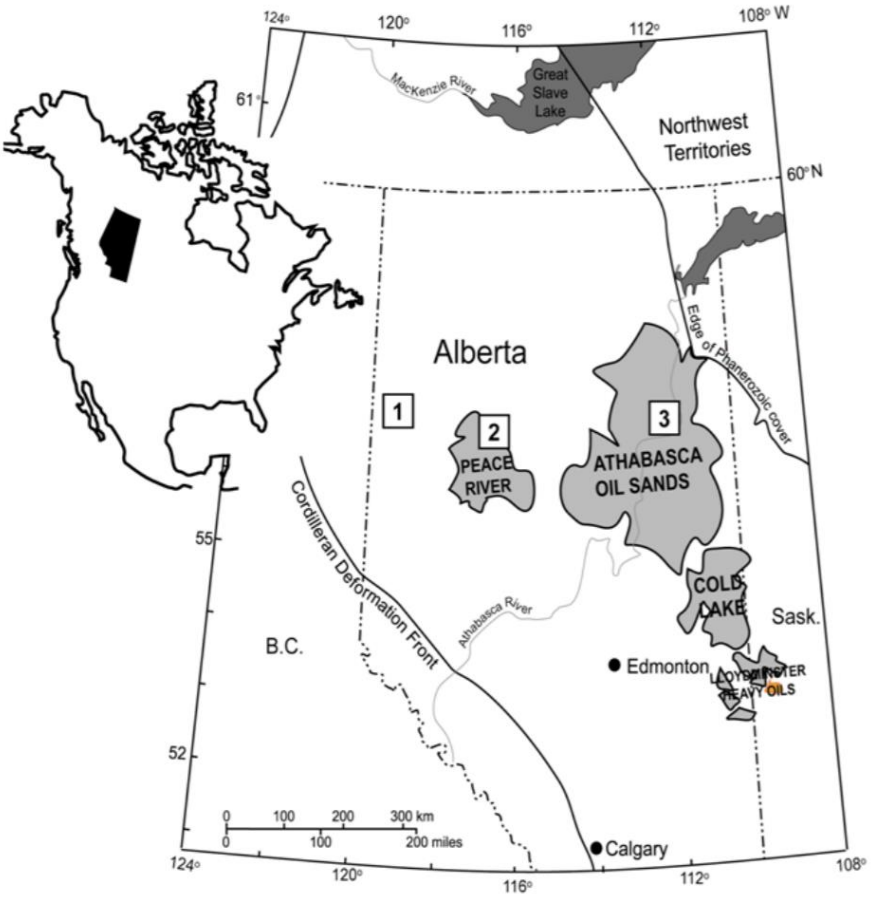

Figure 1.3: Oil sand deposits of Canada (Huang & Grasby, 2015)

1.1 Importance of clay shale caprock

Clay shale caprock integrity is essential to the success of thermal recovery processes and in-situ operations (Oldakowski et al., 2016). The primary role of caprocks is to act as a sealer for injected steam and other fluids in such operations.

Therefore, caprocks should retain a low permeability and remain strong to provide a mechanically strong seal under high temperature and pressure operations. Limited information is available on mechanical and physical changes that occur when temperature and stress conditions change nearby caprock. Understanding these changes could help to calculate maximum allowable pressure during recovery, which could improve the economics of such operations.

1.2 Physical and mechanical properties of clay shale

The physical and mechanical properties of clay shales are of interest in many fields such as geotechnical engineering, geophysics, petrophysics, etc. The material's physical properties are defined as characteristics of the sample that can be measured without the change of state (Štubňa et al., 2018). Some examples of physical properties include colour, weight, and density. On the other hand, the mechanical properties of clay shales are defined as the response of the sample to external loads (Zouaoui & Bouaziz, 2017). Young's modulus, Poisson's ratio and shear strength are some examples of mechanical properties.

Clay shales are composed of different mineral grains or crystal structures, as shown in Figure 1.4. Ding (2020) presented the mineral and clay composition of five different samples using XRD and scanning electron microscopy (SEM). Thus, considering the complex structure of clay shales, they are driven by their main constituents and affected by several factors. According to Li et. al. (2016), some of the factors include:

- Water content and salinity: increased content weakens the rock strength by increasing pore pressure and decreasing the effective stress.
- Orientation of the bedding plane: perpendicular to bedding has higher unconfined compressive strength than the parallel bedding planes.
- Total organic carbon (TOC): increase in TOC weakens the geomechanical behavior.
- Clay content: clay-rich rocks display ductile mechanical properties, and clay deficient rocks are brittle. Therefore, Young's modulus decreases with an increase in clay content.
- Porosity: a larger porosity increases the Poisson's ratio and decreases the Young's modulus
- Temperature: high temperature of clay shales weakens the shale strength. Young's modulus, tensile and compressive strength decrease with increasing temperature.

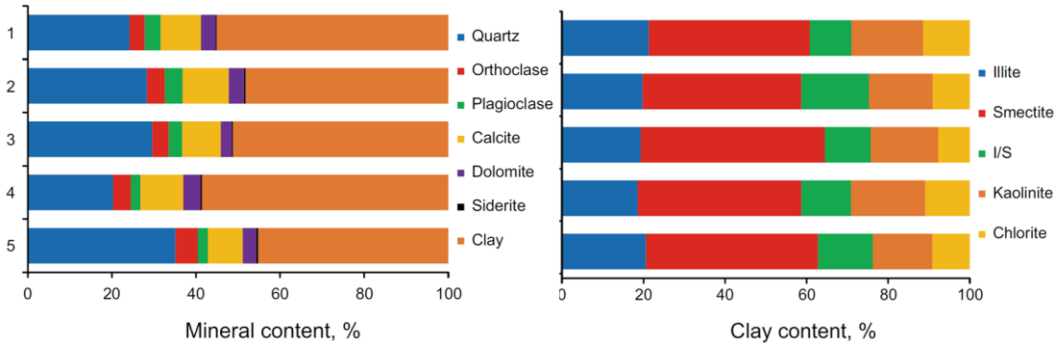

Figure 1.4: Clay shale and mineral composition in upper Triassic reservoir (Mazouz et al., 2020)

1.3 Methods to determine physical and mechanical properties of clay shales

There are many methods and techniques in use to determine clay shales' physical and mechanical properties (Boulin et al., 2012; Geng & Sun, 2018; Mohajerani et al., 2014; Štubňa et al., 2018; Tian et al., 2014). Confined triaxial compression testing is one of the most common methods to determine rock-mechanical properties (Amšiejus et al., 2009). The testing is conducted by applying stress to the sample with the confining stress and shearing it to failure to determine the shear strength parameters of the sample. Principal parameters obtained from confined triaxial compression tests are the angle of shearing resistance ϕ (friction angle), shear stiffness *G*, cohesion c', Young's modulus *E*, Poisson's ratio ν, and others (Banerjee et al., 2018; Kim & Kim, 2007; Minaeian et al., 2017).

Figure 1.5 provides an illustrative sketch of the types of triaxial tests required for a given section of a slope. Based on Figure 1.5, the compression test is preferred near the top due to the failure mechanism being dominated by friction. However, soil mainly fails under tension at the bottom of the slope. Therefore, it is preferential to conduct a triaxial extension test for the bottom of the slope.

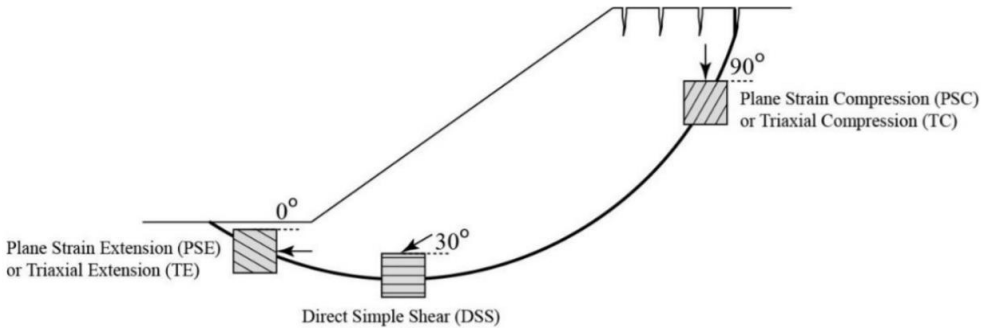

Figure 1.5: Engineering practice of triaxial compression test (Abed & Korkiala-Tanttu, 2018)

Besides testing the shale, is also essential to understand the mineralogical component of the shale. The mineralogical analysis of clay shales has been broadly determined using X-ray Diffraction (XRD) and X-ray fluorescence (XRF) techniques (Geng & Sun, 2018; Guo et al., 2020; Ouahabi et al., 2015; Sun et al., 2016).

XRD is a non–destructive technique that allows us to analyze mineral properties such as phase composition, lattice parameters, crystalline structure, and many more powdered samples obtained from reservoir (Fontaine et al., 2018). Moreover, when measured at various and non-ambient temperatures, phase transformation, reaction processes, crystalline growth, dehydration, and oxidation can be evaluated (Castellanos et al., 2012; Fontaine et al., 2018). Morodome and Kawamura (2009) performed XRD analysis on montmorillonite clays as shown in Figure 1.6. XRD pattern shows that the tested clay shale sample has a high content of montmorillonite. Considering the high susceptibility of it to change under high temperature it is important to understand the effect of heat on clay as a composite.

Authors have reported that the maximum peak intensity has decreased gradually with the increase in temperature.

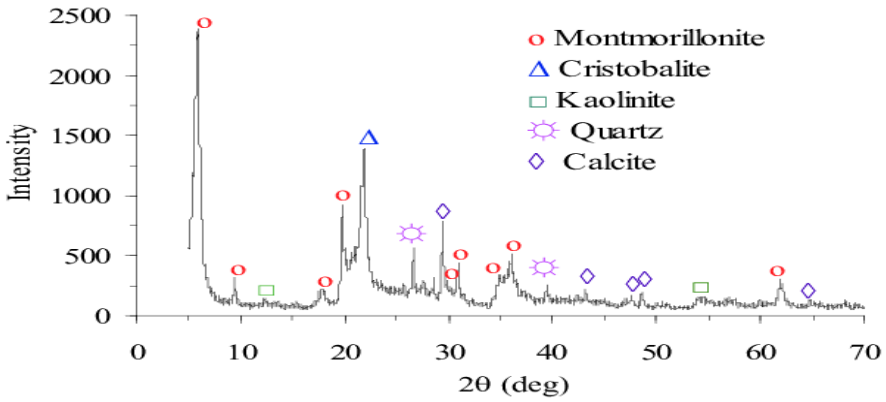

Figure 1.6: X-ray diffraction pattern of a montmorillinitic clay (Morodome & Kawamura, 2009)

XRF is another common method used in composition analysis, where it is used to identify the elemental composition of materials. However, it does not indicate phases present in the sample (Hazra et al., 2016). XRF determines the chemistry of a sample by measuring the fluorescent X-ray emitted from a sample (Johnson et al., 1999). Every element produces its own unique fingerprints. XRF can differentiate and provide the elemental composition (Hazra et al., 2016). Therefore, XRF spectroscopy is an excellent technology for qualitative and quantitative analysis of material composition. Table 1.1 shows the chemical composition obtained by the XRF technique on clay cores obtained from Xuzhou of Jiangsu Province, China (Geng & Sun, 2018). Its chemical composition indicates the presence of silica and alumina as major constituents, along with traces of

hematite, sodium oxide, potassium oxide, calcium oxide, magnesium oxide, and Loss on Ignition caused from volatile materials lost in the sample.

Table 1.1: Chemical composition obtained by XRF technique on clay (Geng & Sun, 2018)

Chemical analysis	Al_2O_3	SiO_2	Fe_2O_3	Na_2O	K_2O	CaO	MgO	LOI
Content (%)	34.64	55.34	1.92	0.16	1.31	0.22	0.31	6.1

1.4 Research motivation

High temperature treatment tests are conducted on clay shale caprocks to investigate and resolve some of the long-established issues related to rocks specific mechanical and mineralogical characteristics. One of the main objectives of laboratory based experimental rock mechanics studies is to assess deformation and strength properties of the shale. This could be achieved by applying different stresses imitating in-situ stress conditions of the underground geological formation (Minaeian et al., 2017).

Previous studies addressed this issue by applying conventional triaxial compression tests at varying confining pressures on cylindrical core samples (Amšiejus et al., 2009). These studies contributed a lot to the development of unconventional wells, as well as other underground operations (Boulin et al., 2012; Motghare & Musale, 2017; Oldakowski et al., 2016; Sun et al., 2016; Yan et al., 2017; Zou et al., 2012). In these cases, most of the rocks mechanical properties could be related to in-situ conditions. However, majority of these studies do not

take into consideration high temperature changes, which can alter its microstructural characteristics (Tian et al., 2014).

Furthermore, clay shale exposed to high temperatures would have different parameters from those tested at ambient temperature. Numerous studies have been conducted at high temperatures, either at room temperature with slow heating or under high temperatures (up to 900 °C) to analyze the effect of high temperature on parameters of clay shale (Geng & Sun, 2018; Guo et al., 2020; Mohajerani et al., 2014; Sun et al., 2016; Tian et al., 2014). However, they lack comparison between two heating conditions, where clay shale properties can significantly depend on temperature. Additionally, these properties are function of initial rock conditions and loading conditions.

Moreover, in the last decade, considerable amount of researches have been conducted studying the effect of high temperature for sedimentary rocks and crystalline rocks (Chen et al., 2017; Nicksiar & Martin, 2013; Sygala et al., 2013). However, limited data are available for argillaceous rocks such as mudstone and claystone.

It is vital to have deep understanding on the above-considered issues and broaden the accessible data on argillaceous rocks. Therefore, this study focuses on investigating the effects of pre-heating and cooling on physical and mechanical properties of clay shales (cap rocks).

1.5 Thesis outline

This dissertation consists of five chapters.

In Chapter 1, introductory topics such as: importance and benefits of studying clay shales and their constituent physical and mechanical properties. In addition, background information on the geological setting of the site from where samples provided are explained.

In Chapter 2, previous experimental studies on physical and mechanical behavior of caprocks and their temperature dependence are reviewed and analyzed in detail.

In Chapter 3, descriptions of testing setup as well as the implemented experimental programs and procedures are outlined.

In Chapter 4, results of the extensive series of thermo-mechanical experiments on Wabiskaw member clay shales presented. Changes in physical and mechanical behavior are discussed thoroughly.

Lastly, in Chapter 5, conclusive remarks as well as number of recommendations for future development of this study are presented.

Chapter 2

2 Literature review

2.1 Introduction

Over the next few decades, global energy demand will grow significantly (Matsou et al., 2013; Huang 2014). This is due to the projected increase in world population combined with industrial, and technological advancements in developing countries. Currently, most of the countries' energy consumption mainly relies on conventional reservoirs. However, the depletion of conventional reservoirs requires more reliance on unconventional reservoirs (Favero et al., 2018). Despite having vast reserves, unconventional reservoirs are economically and technically challenging (Holditch, 2013; Hongjun et al., 2016). Unconventional reservoirs, with their respective challenges, can be found at various depth locations. One challenge of exploring these reservoirs is the low permeability with high fluid viscosity. Thermal operation is one of the most common industrial solutions for these challenges (Chang et al., 2013; Florez & Gildin, 2019). Two major implemented in-situ thermal operations are steam-assisted gravity drainage (SAGD) and in-situ combustion (Pugsley et al., 2013; Rahnema et al., 2017; Shi et al., 2017; Xia et al., 2003). Considering both methods imply heat application, the shale caprocks undergo high-temperature treatment. Additionally, injection of steam or other fluids will impose new mechanical loads onto shale. Therefore, clay shale layers will be under different thermo-mechanical conditions (Motghare &

Musale, 2017; Yan et al., 2017; Zou et al., 2012). Consequently, microstructures of clay shales may change through the formation of new micro-cracks or disturbance of the pre-existing cracks or mineral transformation (Favero et al., 2018). Further, this will alter the physical and mechanical characteristics of shale. Therefore, it is vital to understand the change in rock-mechanical behaviors of clay shales due to imposed thermo-mechanical loading. A series of studies were conducted to analyze the behavior of these parameters at varying temperatures and confining pressures by imitating in-situ conditions (Boulin et al., 2012; Geng & Sun, 2018; Motghare & Musale, 2017; Oldakowski et al., 2016; Sun et al., 2016; Yan et al., 2017; Zou et al., 2012).

2.2 Effects of thermal treatment on clay shale physical properties

Numerous studies have shown that the physical properties of clay shales have a high dependency on temperature (Boulin et al., 2012; Masri et al., 2014; Mohajerani et al., 2014; Sun et al., 2016; Zhang et al., 2014). These studies attempted to explain possible causes of clay's physical properties due to thermal heating. Some of the properties studied include apparent shape, mass, bulk density, and the mineral transformation of clay shales. These studies improved rock mechanics analysis for constantly evolving industrial operations.

2.2.1 Apparent shape

When a specimen is treated at high temperatures, it does not only change its apparent features (such as color). However, it may also undergo external changes such as volume expansion and cracks (Hajpál, 2002). The volume expansion and change in apparent features are caused by the physical and chemical changes with temperature and pressure. It is important to understand the knowledge of volume expansion and thermal crack formation in many applications, involving analysis of wellbore stability, construction, and integrity assessment of caprocks for enhanced oil recovery (EOR) through thermal treatment.

2.2.2 Volume, mass, and bulk density

Previous studies on clay shale physical properties at high temperatures indicate that the density changes of a specimen are mainly associated with its mass and volume change (Ding et al., 2009; Geng & Sun, 2018; Han et al., 2017). The weight loss is mainly due to the evaporation of water content and the disintegration of carbonates (Tian et al., 2012). Based on numerous studies, during thermal treatment, water incorporated in clay shales experience significant state changes (Ding et al., 2009). For instance, adsorbed water on the clay surface, interlayer and structural waters contained in clay tend to escape at various temperatures (Han et al., 2017). Following the previous experiments, the adsorbed water evaporates around 100℃, the interlayer water evaporates within 100℃-250℃, structural water escapes, and dihydroxylation of organic materials occurs at temperatures above 300℃-400℃ (Geng & Sun, 2018; Guo et al., 2020; Sun et al., 2016). Further, during laboratory experiments, Han et al. (2017) and Sun et al. (2016) analyzed

clay samples from Xuzhou, China. The authors observed a total mass loss of around 2.5% after heated up to 800℃. The significant mass loss occurred below 150℃ by evaporation of adsorbed water. Between 300℃-500℃, mass losses mainly consisted of dissipation of structural waters with oxidation and decomposition reactions of hydrocarbons, leading to the rest of 24% the total weight loss. Above 500℃ no significant changes were noticed.

Additionally, volume increment in clay shales mainly occurs due to thermal expansions and crack openings above 800℃ by permanent expansion after cooling down (Tian et al., 2012).

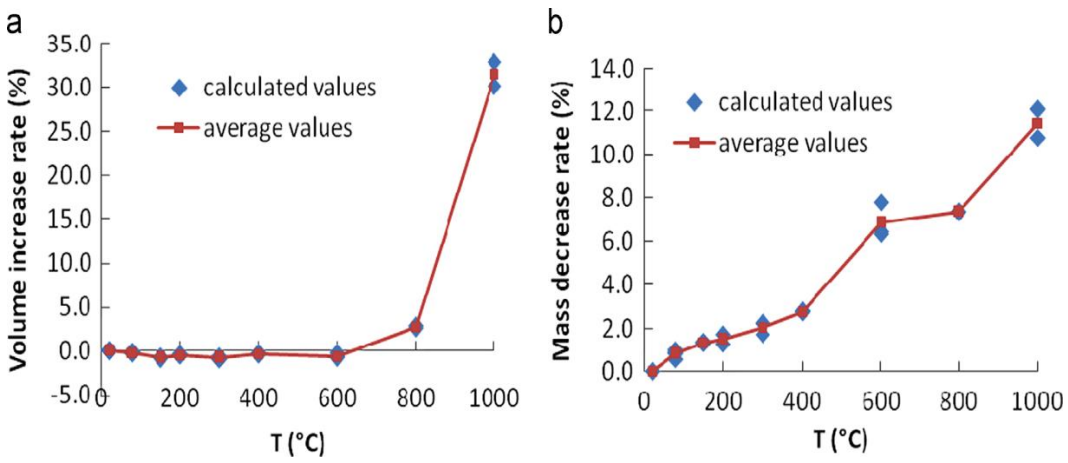

Figure 2.1: (a) Volume increase rate vs temperature of clay shale; (b) Mass decrease rate vs temperature of clay shale (Tian et al., 2014)

Figure 2.1 illustrates the effect of high temperature on the volume and mass of a clay shale specimen (Tian et al., 2014). A negative value in volume increase rate is observed before 600℃ (Figure 2.1 a). Tian et al. (2012) relate this to the shrinkage of clay minerals and closure of pre-existing micro-cracks at relatively low temperatures. Even though volume decreases below 600℃, weight loss rate

increases significantly (Figure 2.1 b), resulting in lower densities. Amount in volume increase rate hikes substantially after 600℃ compared to mass loss, producing even lower densities. Similar results were observed by other authors (Hongjun et al., 2016; Húlan et al., 2015).

2.2.3 Crack formation

Volume expansion and crack formation rate in clay shales can be influenced by many factors: mineralogical composition, texture, pressure, temperature, porosity, pre-existing micro-fractures, and pore fluid properties (Gabova et al., 2020; Siegesmund et al., 2000). Further, micro-cracks caused by temperature change may coalesce and larger cracks can form. This then leads to a change in the elastic moduli of the sample (Grebowicz, 2014).

Tian et al. (2014) conducted an experimental analysis on six clay samples at different temperatures ranging from ambient temperature to 1000℃ as shown in Figure 2.2. Based on their observations at 1000℃, the clay sample was cracked or even failed. It can be observed from the figure that at the highest temperature, the clay failure was accompanied by irregular longitudinal cracking causing a significant decrease in strength. The authors related this failure due to the clay lithology, anisotropy, brittleness, initial rock microstructures and applied confining stresses.

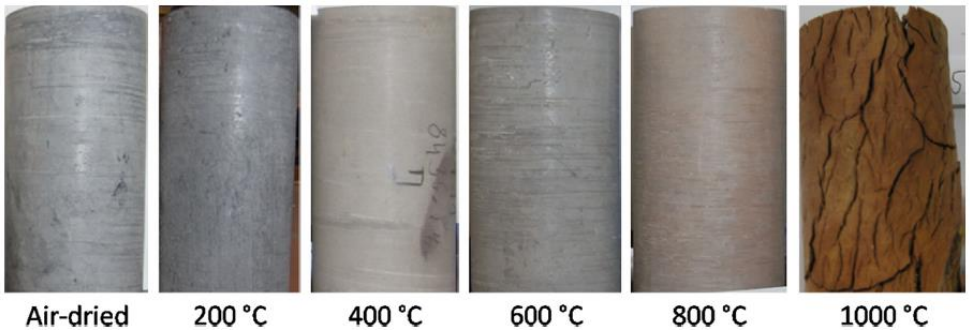

Figure 2.2: Claystone specimen after treatment at different temperature ranges (Tian et al., 2014)

2.2.4 Minerals transformation

High temperature treatment on clay shales involves alteration processes of the structure, which leads to changes in physical and mechanical characteristics. Main challenge is to predict the phase transformations of minerals due to the changes in physical and mechanical characteristics of clay shale with temperature. As a result, researchers effortlessly investigate microstructure property, compositions, and processing relationships for clay shales, by using XRD and XRF techniques (Miras et al., 2018).

XRD examines the crystalline/semi-crystalline structure of materials through its comparable scattering X-ray wavelengths (Miras et al. 2018). The interatomic spacing of observed crystalline solids provides a qualitative representation of atomic arrangements within lattice planes (Rajeswari et al., 2020). Ouahabi et al. (2015) investigated mineral modifications of four calcareous clays (Figure 2.3) using the XRD technique at varying temperatures of up to 1100℃. They observed that carbonate clays were rich in illite and kaolinite minerals with large amount of quartz compared to K-feldspar, plagioclase, dolomite and calcite.

Overall, significant mineralogical changes were observed in the samples at temperatures ranging from 800℃ to 1100℃. After 950℃, phyllosilicates disappeared by modifying onto spinal and calcite with the reaction of other minerals. The decomposition of calcite and dolomite into lime occurred around 1100℃. Then, they reacted to form new calcium minerals, such as plagioclase, gehlenite, hematite and wollastonite. Quartz was preserved throughout the experiment, while K-feldspars disappeared at temperatures below 1000℃.

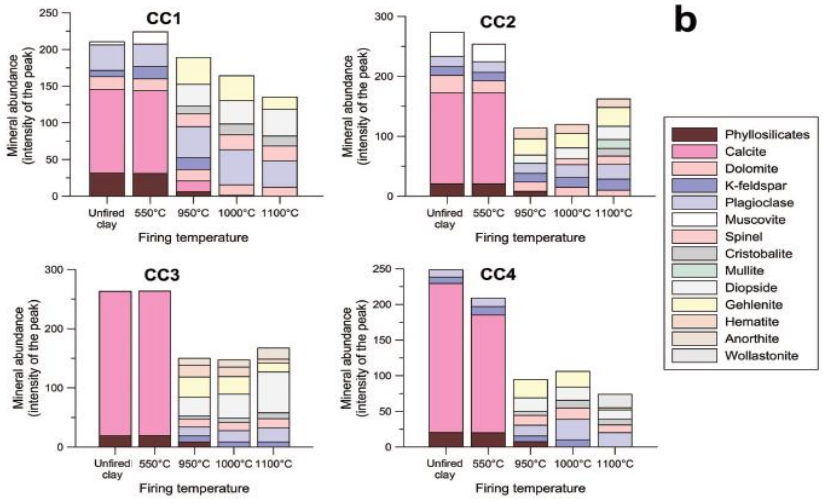

Figure 2.3: Mineral composition of four calcareous shales at varying heating temperatures (Ouahabi et al., 2015)

Similar results were obtained by Miras et al. (2018) by heating two clay specimens at temperatures ranging from room temperature up to 1000℃. Further, below 600℃, no substantial mineralogical modifications were detected. Besides, dihydroxylation of kaolinite and improvement of the bond between particles at this range occurred, which also agrees with the results of Han et al. (2017) and Štubňa et al. (2018). However, dolomite was fully decomposed at 740℃, forming identical

modified phase minerals. In contrast, Ouahabi et al. (2015) reported that the existence of dolomite was noticed throughout the experiment. Similar results were also obtained by Gunasekaran and Anbalagan (2007), where dolomite decomposition started at 600℃ and disappeared at 750℃. Though many researchers mentioned the presence of high temperature calcite phases such as larnite and wollastonite (Ouahabi et al., 2015; Trindade et al., 2010), Miras et al. (2015) did not find them in their study. Table 2.1 below displays clay minerals and their reaction types at various temperatures, summarized from the works of various authors (Geng & Sun, 2018).

Table 2.1: Clay mineral reactions at different temperatures (Geng & Sun, 2018)

Temperature (°C)	Mineral	Reaction
25–220	Ca-Montmorillonite	Desorption
25–220	Mg-Montmorillonite	Desorption
400–695	Mg-lllite	Decomposition
455–642	Kaolinte	Decomposition
554–723	Ca-Montmorillonite	Decomposition
573	Quartz	α-β inversion
700–800	Calcium carbonate	Decomposition
790–950	Mg-lllite	Decomposition
816–908	Ca-Montmorillonite	Decomposition
300–500	Organic matter	Oxidation and carbonization
400–800	Carbon	Oxidation

Besides the XRD technique, XRF is also one of the most common techniques used to determine the mineralogy of clay shales. The XRF technique determines the chemical composition of a clay shale without identifying the phase changes. In contrast, QXRD can determine the presence and amount of minerals in clay shale and phase change identification (Zhang et al., 2014). Therefore, XRF is

essential to determine the effect of thermal treatment on the elemental composition of a clay shale (Hupp & Donovan, 2018). Many researchers have conducted an XRF test to investigate the effect of the thermal treatment on the mineralogical composition of clay shale (Amer et al., 2019; Geng & Sun, 2018; Zhang et al., 2014). The mineral composition of two different oil shales was presented in Table 2.2 (Amer et al., 2019). As can be seen from obtained XRF analysis, silica, alumina, hematite, sodium oxide, calcium oxide, and magnesium oxide are the most common components of clay shales (Amer et al., 2019; Geng & Sun, 2018, 2018; Hazra et al., 2016; Zhang et al., 2014).

Table 2.2: XRF analysis of El-Lajjun and Al-Mahata oil shales (Amer et al., 2019)

Component	EL %	IA %
SiO_2	18.3	17.6
Al_2O_3	3.12	3.65
TiO_2	0.35	0.39
Fe_2O_3	1.78	1.52
CaO	31.6	35.5
P_2O_5	3.63	1.92
LOI	41.2	39.1

The shale minerals tend to undergo different phase transformations, and carbonates decompose, reaching their critical value at high temperatures. This affects clay shale characteristics such as compressive strength and elastic modulus. This will be further discussed in later parts of this thesis.

2.3 Effect of thermal treatment on clay shale mechanical properties

Due to their low permeability, clay shales are a great cover or a barrier for geological formations. In the case of heavy oil formation, where shales act as a caprock, it is crucial to have a detailed knowledge of their thermo-mechanical behavior (Mohamadi & Wan, 2016). During thermal operations such as SAGD operation, high-temperature steam is injected into the reservoir formation to generate thermo-mechanical loads and high fluid pressures on caprock shales, potentially leading to material damage (Sarmiento, 2021). As a result, integrity of shale, which should act as a hydraulic seal for steam injection will be compromised. Also, in some cases, shales can act as a reservoir formation (Aguilera, 2016). However, enhanced oil recovery (EOR) or hydraulic fracturing methods are required to increase the permeability to produce from these formations. Nevertheless, in all cases shales are subjected to a high pressure and complex thermo-mechanical loads (Masri et al., 2014). Therefore, it is vital to study and investigate their mechanical characteristics to evaluate their durability and integrity at elevated temperatures and pressures. Some factors include compressive strength, cohesion, friction angle, fracture mode, Young's modulus and Poisson's ratio.

2.3.1 Mechanical strength

Confined triaxial compression testing is one of the most common methods used to measure the mechanical properties of deformable rocks (Minardi et al., 2021). The key advantage of this method with respect to in-situ conditions is its

ability to measure effective stresses and volumetric strains by applying uniform confining and axial loads, which is essential to understand the entire nature of the rock failure.

Numerous researchers have attempted to examine mechanical properties of clay shales by conducting laboratory experiments at various temperatures and confining pressures to simulate the original geological conditions (Oldakowski et al., 2016; Sun et al., 2016; Tian et al., 2014).

One of the important mechanical properties gained from triaxial testing is shear strength (Han et al., 2017). A rock can resist shear stresses imposed on the rock (Das & Sivakugan, 2015). The shear strength of a clay shale can be obtained by performing at least two conventional triaxial tests and drawing the Mohr's circles. This allows to assess two shear strength parameters: cohesion and friction angle (Laloui & Loria, 2019). Cohesion is the shear strength at zero net compressive stress, which is independent of interparticle friction. It is the force which keeps particles together. Whereas friction angle is the shear resistance of interlocked particle against applied normal effective stresses (Muniz et al., 2005; Patil et al., 2017).

Liu et al. (2020) tested thirty-nine core samples retrieved from under varying minor and major principal stress conditions. Figure 2.4 illustrates the identification of Mohr circles obtained under large variable confining pressure with the maximum of 140 MPa. The authors identified variation of cohesion force and internal friction angle with confining pressure.

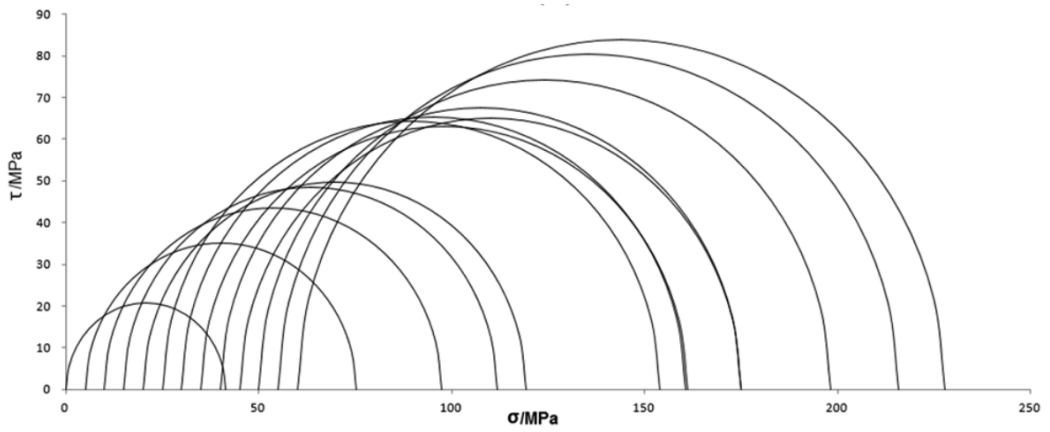

Figure 2.4: Mohr's circle of tight sandstone of (Liu et al., 2020)

Throughout the previous studies, it has been found that elevated temperatures highly affect shear strength. For example, (Kosar, 1989) obtained results from triaxial compression tests at temperatures between 20℃ and 225℃ for Clearwater formation shale in Alberta, Canada. The author demonstrated an increase in shear strength at higher temperatures. In contrast, Ibanez and Kronenberg (1993) found an opposite trend for Wilcox shale at the same range of temperature. Chalaturnyk (1996) studied the Upper and Lower McMurray shale (a mixture of oil sand and shale) under a confined triaxial compression test at 20℃ and 225℃. Findings indicated a decline in shear strength with temperature for Upper and Lower McMurray shales. Okada (2005) published results of triaxial compression tests at 20℃ and 60℃ for mudstone, which confirmed a weakening of shale samples with temperature. Masri et al. (2008) also confirmed a decrement in shear strength with temperature for Tournemire shales through confined triaxial compression tests at five different temperatures ranging from 20℃ and 225℃. Mohamedi and Wan (2016) studied Colorado shale, a cap rock for Westgate and Joli Fou formations in east-central Alberta, Canada. Samples were examined based

on triaxial compression testing between 25℃ and 135℃ temperatures. Results revealed initial strain hardening and densification before the peak deviatoric stress was reached. After that, softening behavior was observed with the increase in temperature. Deviatoric stress is the difference between the effective major and minor principal stresses acting on a specimen.

Furthermore, in some publications, it is identified that rock strength substantially increases with the increase of confining pressures when subjected to high thermal treatments (Jha et al., 2017; Tian et al., 2012). Tian et al. (2014) investigated claystone's strength behavior when exposing it to temperatures up to 1000℃ and varying confining pressures between 0.1 MPa to 20 MPa (Figure 2.5) under the confining triaxial testing. The increment of confining pressures induced a non-linear increment (2 - 5 times) of peak strength within the range of 25℃ to 800℃. Afterwards, a sharp decline in strength occurred, reaching 40% of room temperatures peak strength at 1000℃, irrespective of applied confining pressures. dividing the thermal treatment process into three stages. The main factor of shear strength's increase below 200℃ was due to the micro-crack closure caused by produced thermal stresses with temperature. Sample strengthening occurred at a temperature above 800℃. This occurred due to the transformation of minerals such as dihydroxylation of kaolinite and inversion of quartz. The development of significant micro and macro fractures was the main reason for the weakening of claystone at 1000℃.

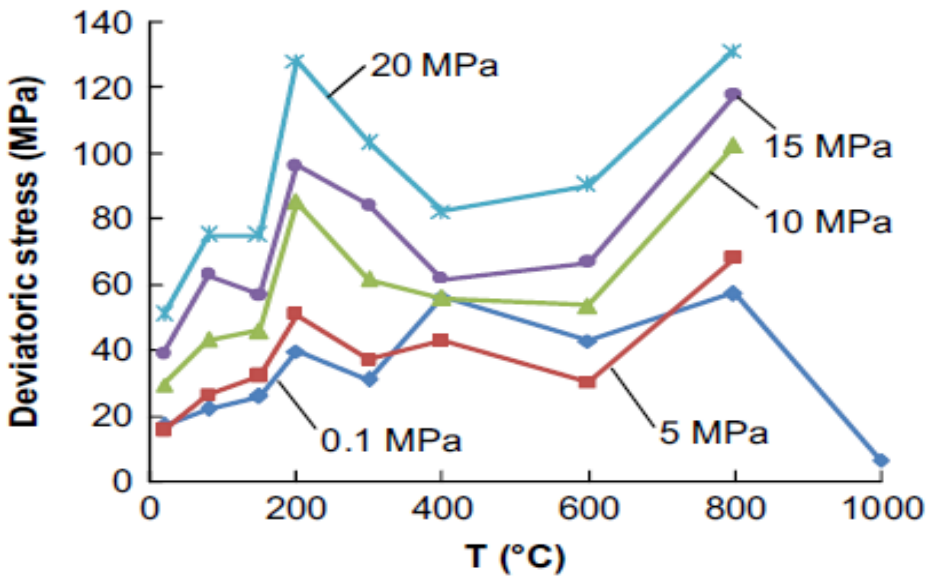

Figure 2.5: Variation of rock strength with temperature at different confining pressures (Tian et al., 2014)

Jha et al. (2017) investigated the effect of high temperature on clay shales without confining pressure through experimental analysis on clay shales of the upper Vindhyan basin in India, treating at temperatures up to 900℃. The continuous decline was observed in compressive strength from 63.45 MPa to 18.45 MPa at temperatures of 25℃ and 900℃, respectively. The authors concluded that the main factor for this significant change is thermal damage or deformation of the sample induced by the increase in temperature. Such damage can have an adverse effect on the physical and mechanical properties of clay shale. Same as Tian et al. (2014) and Jha et al. (2017) explained it by dividing it into three regions. However, explanations were quite controversial. In the first region (till 200℃), because of evaporation of moisture and openings of pre-existing cracks compressive strength of shale declined sharply. A decrease in strength occurred in the second region (till 600℃). The authors attributed it to the temperature effect on further crack

enlargement, weakening grain particle bonds. Shale samples were totally damaged at temperatures above 600℃, resulting in a lower compressive strength.

From the above-mentioned previous studies, it seems that there are some inconsistencies regarding interpretations of mechanical strength properties of clay shales as a factor of high temperatures. Given the importance of shale properties, more detailed studies are needed to examine caprock's strength on the effects of elevated temperatures.

2.3.2 Elastic properties

The elastic properties of clay shale are important mechanical characteristics alongside with shear strength. The elastic modulus of the linear elastic deformation respond of clay shale under deformation, and it can be determined from unloading and reloading cycles during laboratory experiments (Radovic et al., 2004). It can be described by its two basic properties: Young's modulus (elastic moduli) and Poisson's ratio. Young's modulus is the stiffness of a material in the elastic region that deformation recovers after unloading. It can be determined from the tangent slope of the elastic region before the peak strength of stress-strain curves, as shown in Figure 2.6. On the other hand, Poisson's ratio measures the deformation of a material in a section perpendicular to the applied force's direction (Belyadi et al., 2017). It is calculated as the ratio between the radial and axial strains during the elastic region before the peak strength of the stress-strain curves (Masri et al., 2014).

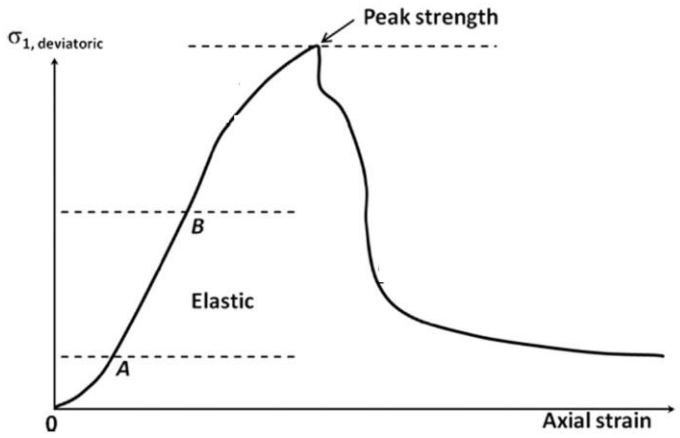

Figure 2.6: Typical stress-strain curve for rocks under triaxial compression test (Tian et al. 2014)

Extensive research was conducted on elastic modulus, and they were mainly divided into two stages:

i) At ambient temperature

Favero et al. (2018) investigated the elastic properties of Opalinus clay shale for confining pressures ranging from 2 MPa to 12 MPa. Results indicated higher Young's modulus at higher confining pressures. However, the rate of increment slowly decreased as the confining pressure increased. Giger et al. (2018) studied the impact of effective mean stress on elastic properties of Opalinus clays based on confined triaxial compression tests. Until the peak, a high direct dependency of Young's modulus on effective mean stress was observed. In contrast, Giger et al. (2018) did not notice a direct relationship of effective mean stress to Poisson's ratio. Similar results were observed by Minardi et al. (2021) during the investigation of Opalinus clay. Elastic moduli were positively correlated with mean effective stress, while Poisson's ratio decreased with increasing stress.

ii) From ambient to higher temperatures

Masri et al. (2014) analyzed the effect of high temperature ranging from 20℃ to 250℃ on elastic properties of Tournemire shale at 5, 10 and 20 MPa confining pressures under triaxial compression tests. As a result (Figure 2.7), Young's modulus increased substantially with the increasing confining pressure up to 10 MPa and continued at a lower rate until 20 MPa. However, elastic moduli decreased with the increasing temperature from ambient to 250℃. The authors have concluded that compaction and expansion of bedding planes leading to a ductile behavior could be the main factor in elastic modulus change. Moreover, Masri et al. (2014) determined Poisson's ratio of shale. As the decrease of Young's modulus occurred with increasing temperature, Poisson's ratio increased as temperature was raised to 250℃ from the ambient temperature. This was due to enhanced deformability and ductility of shale with temperature.

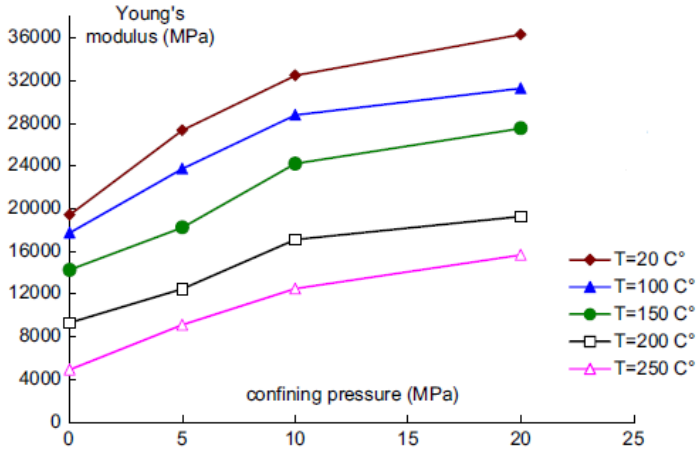

Figure 2.7: Young's modulus vs confining pressure at different temperatures (Masri et al., 2014)

Tian et al. (2014) investigated deformation modulus at 0.1 MPa, 5 MPa, 10 MPa, 15 MPa and 20 MPa confining pressure as a function of treatment temperature from ambient to 1000℃. The deformation modulus of the claystone exposed to high temperatures up to 800℃ are higher than those at ambient temperature, where the samples totally failed at the temperature above 800℃. Like Mires et al. (2014), Tian et al. (2014) also noticed identical patterns of deformation modulus variations with temperature under different confining pressures. Tian et al. (2014) also observed a positive effect of confining stress on Young's modulus. The higher the confining stress, the higher Young's modulus. On the contrary, thermal treatment increased Young's modulus significantly until 200℃ for all confining stresses. At higher temperature, parameters followed a steady trend with a small increments and decrements until 800℃.

Similar results were also obtained by Oldakowski et al. (2016) in the analysis of caprock from Wabiskaw Member of Clearwater Formation at Athabasca oil sands. Shale samples were tested from room temperature (25℃) until 200℃ at varying low confining pressures up to 1.3 MPa under triaxial compression testing. Results indicated strong dependence of Young's modulus on confining pressure. Oldakowski et al. (2016) drew a linear straight fit between Young's modulus and confining pressure. However, compared to Miras et al. (2014), Oldakowski et al. (2016) did not notice any relationship between Poisson's ratio and confining pressure within the studied temperature range.

In the same way, Mohamadi and Wan (2016) observed an increase in Poisson's ratio from room temperature to 85℃ and a decrease up until 135℃ for

Colorado shale (caprock). The interrelation of Poisson's ratio with temperature was quite complicated. Hence, the authors could not define any conclusion on how it behaves with temperature. Mohamadi and Wan (2016) presented the same results as previous authors on how Young's modulus increases with confining pressure and decreases at elevated temperatures.

Štubňa et al. (2018) investigated the elastic properties of Estonian clay by heating and cooling the specimens at 900℃, 1000℃ and 1100℃. They noticed that the release of bound water (dehydration) at lower temperatures (20℃ - 250℃) made contact between clay crystals closer, which resulted in higher elastic moduli. On the other hand, dehydroxylation (250℃ - 650℃) of illite and kaolinite slightly impacted clay's elastic moduli, meaning that Young's modulus is more dependent on clay's crystal boundary properties (water at the particle–particle interface) than internal mechanical properties of clay minerals. Due to the structural organization of dehydroxylated minerals, Young's modulus increases at higher temperatures above 700℃. Štubňa et al. (2018) also described that Young's modulus of clays reached their lowest values at 900℃ (12 GPa) and 1000℃ (22 GPa). However, heating the sample to 1100℃ increased elastic moduli (40 GPa) significantly due to the formation of a glassy phase. During the cooling process, Young's modulus reached its highest value of 47 GPa at 800℃ as a result of the increment in viscosity of the glassy phase. It decreased substantially below 800℃ as a consequence of formed microcracks.

2.4 Summary

The continuous increase in global energy consumption and decline in available natural resources leads the world to boost the production of unconventional hydrocarbons employing high pressure or high thermal treatments on reservoirs consisting of clay shales. Hence, knowledge of thermo-physical and thermo-mechanical properties of shales is of the utmost importance for the safe and optimum recovery of hydrocarbons. Current literature describes the performed tests at elevated temperatures and pressures on clay shales obtained from different parts of the world. Throughout the literature, there are some inconsistencies on acquired results due to some factors such as mineralogy, microstructure, etc. making it difficult to relate to other clay shale samples. Therefore, this research focuses on the effect of pre-heating and cooling on the physical and mechanical properties of clay shale samples obtained from the Wabiskaw formation.

Chapter 3

3 Methodology

3.1 Geological setting

The clay shale samples used in this case were retrieved from the Wabiskaw formation at a site near Long Lake, Alberta, particularly. As shown in Figure 3.1, the Wabiskaw formation is located between the marine shales of the Clearwater formation and very fine sands of McMurray formation (Cheng et al., 2015). The Wabiskaw and McMurray formations are located at the depth range of 200 m to 950 m (Devriese & Oldenburg, 2016). Moreover, the Wabiskaw formation consists of interbedded black fissile shale, oil sand and heavy oil (Hein, 2015).

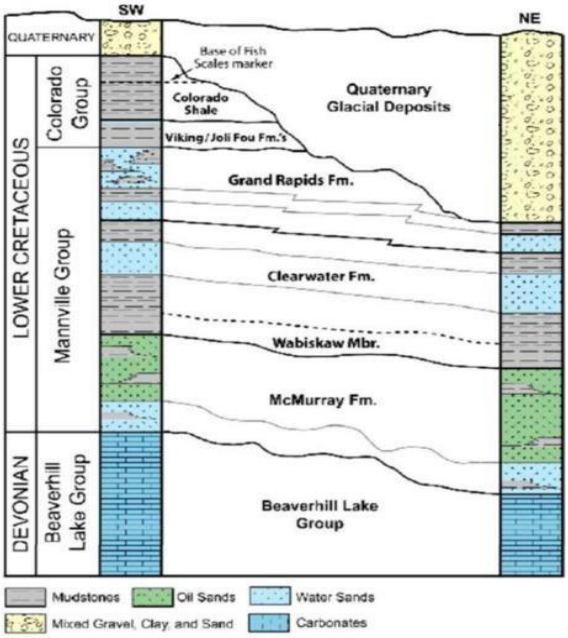

Figure 3.1: Stratigraphic column of the Long Lake area (Cheng et al., 2015)

Heavy oil formations from Wabiskaw member are mainly extracted using thermal recovery processes. One of the most common methods applied are cyclic steam stimulation and steam-assisted gravity drainage with in-situ oxygen injection and combustion (Tian et al., 2014).

3.2 Tested material

The samples used in this study were retrieved from the Wabiskaw formation located in Cold Lake. In the field, cores were carefully cut into 1m segments. Further, to maintain the natural moisture content of 12% and avoid mechanical disturbance, samples were sealed with heat shrinkable membranes and preserved inside PVC tubes. A total of 12 samples from preserved tubes were prepared for the experimental procedure. The trimmed sample dimensions were 75 mm in diameter and 170 mm in height.

3.3 Experimental equipment

The samples used in this study were pre-heated using the Carbolite Vertical Split Tube (VST) 12/200 furnace as shown in Figure 3.2. The inner tube of the furnace can accommodate the specimen with maximum outer diameter and length of 110 mm and 200 mm, respectively. The maximum operating temperature of the furnace is 1200℃ using the heating strings (Hu et al., 2011). Experimental setup was controlled using control panel 301 PID as shown in the Figure 3.2.

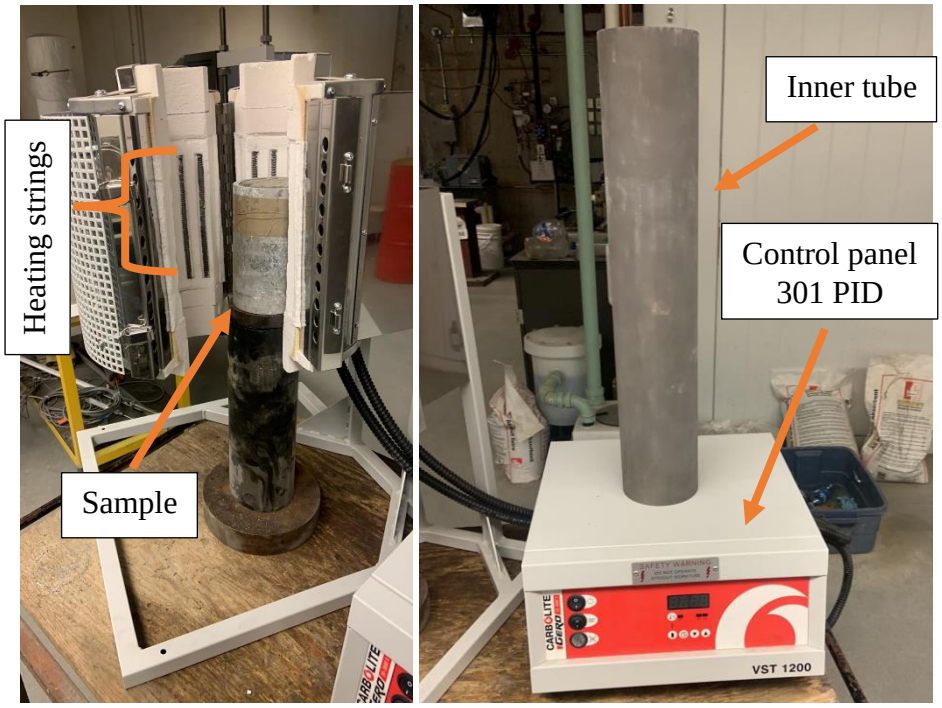

Figure 3.2 Carbolite VST Furnace

Upon completion of heating, samples were naturally cooled down by turning off the heating equipment and waiting for it to cool down to ambient temperature. Thereafter, pre-heated samples were tested using high temperature and pressure GCTS triaxial testing equipment. The triaxial apparatus setup is shown in Figure 3.3. The confining pressure for GCTS equipment was applied using MTS pumps with standard pressure rating of 20.68 MPa. The confining fluid used was a mineral oil and was controlled by PV (Pressure Volume) controller. The circumferential LVDT with a resolution of 1μm was mounted in the middle of the sample with a chain-spring system to measure local radial and volumetric strains, whereas external LVDT is installed to measure axial strains. The direct attachment of the circumferential LVDT to the sample eliminates errors by precisely measuring and detecting local deformities.

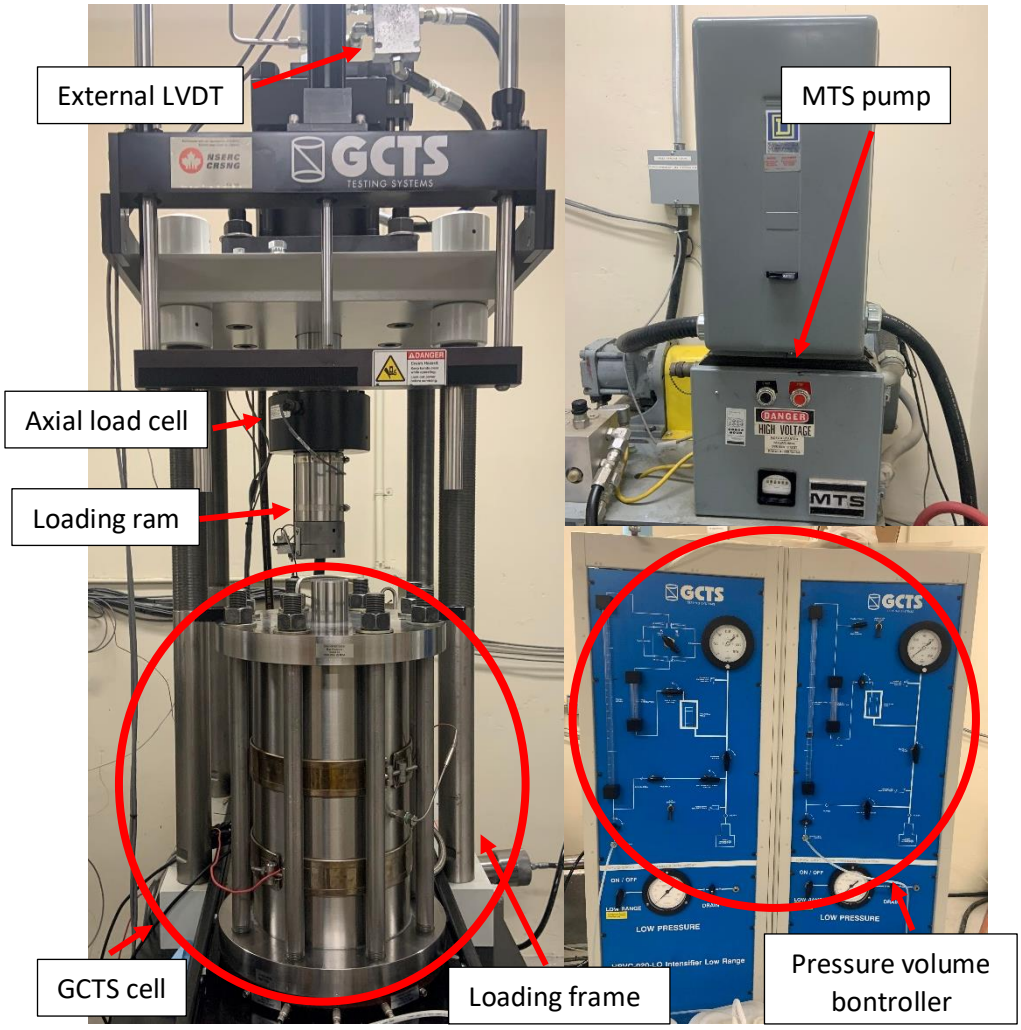

Figure 3.3: Triaxial Apparatus

Furthermore, the mineralogical content of the samples was determined using X-ray Diffraction (XRD) equipment at the University of Calgary. Sample powder was tested in Bragg-Brentano mode as shown in Figure 3.4. The powder was prepared from the sample by hand grinding using mortar and pendle. The scintillation detector regulated the emitted beams of Cu-Kα radiation anode of a diffractometer operating at 200 mA and 50 kV. Graphite monochromator is used to diffract the emitted X-rays of anode. Sample powders were measured with a step

size of 0.02° and scanning rate of 0.95°/minute. Measurements were performed in the 2θ from 3° until 60°.

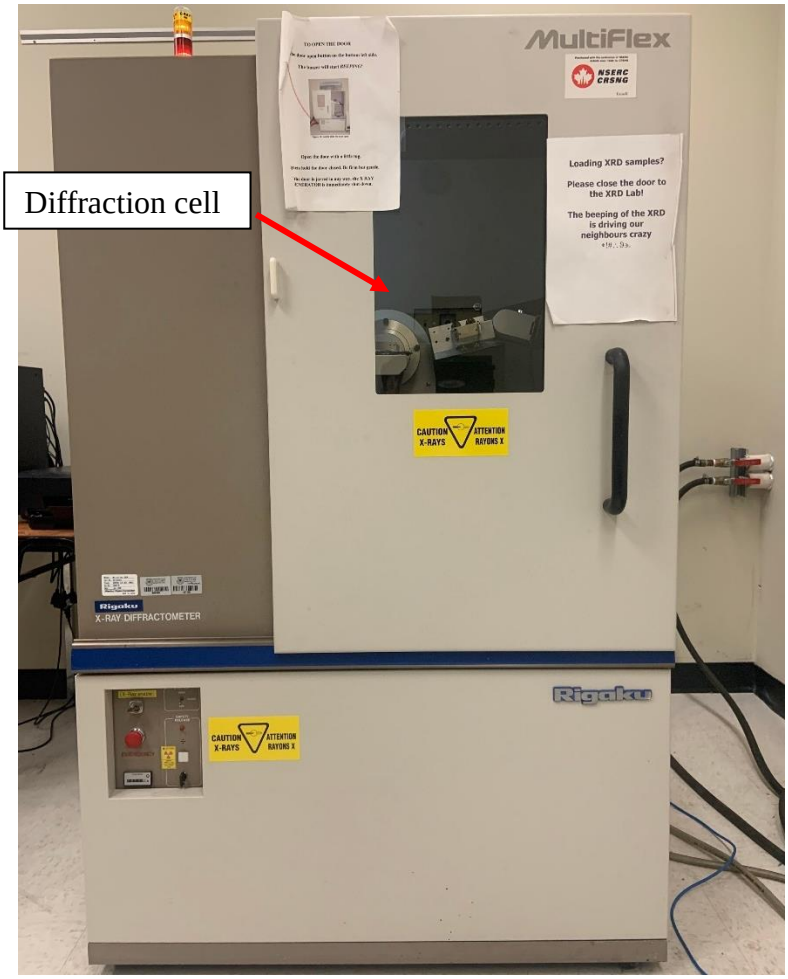

Figure 3.4: X-ray Diffraction (XRD) equipment

In addition to XRD technique, X-ray fluorescence (XRF) technique was used to determine the elemental content of the samples by measuring the fluorescent X-ray emitted from a sample when excited by a primary X-ray source. The powder with weight of 5 grams was prepared and tested by XRF equipment as shown in Figure 3.5.

Figure 3.5: X-ray fluorescence (XRF) equipment

3.4 Thermo-mechanical testing procedure

The following sections explain different stages of experimental procedure in detail. It consists of two main stages: heating and cooling of clay shale samples and, isotropic consolidation and shearing on pre-heated samples.

3.4.1 Heating of clay shale samples

The heating procedure of the samples was classified in three different stages depending on the type of experimentation as shown in Figure 3.6. In total of 12 samples were selected and used for heating stage of this study case. To avoid thermal shock, samples were heated at a rate of 1°C/min using Carbolite Gero at various temperatures ranging from 100°C to 600°C as shown in Table 3.1. Samples were cooled down naturally on its own prior commencing the confined triaxial compression test.

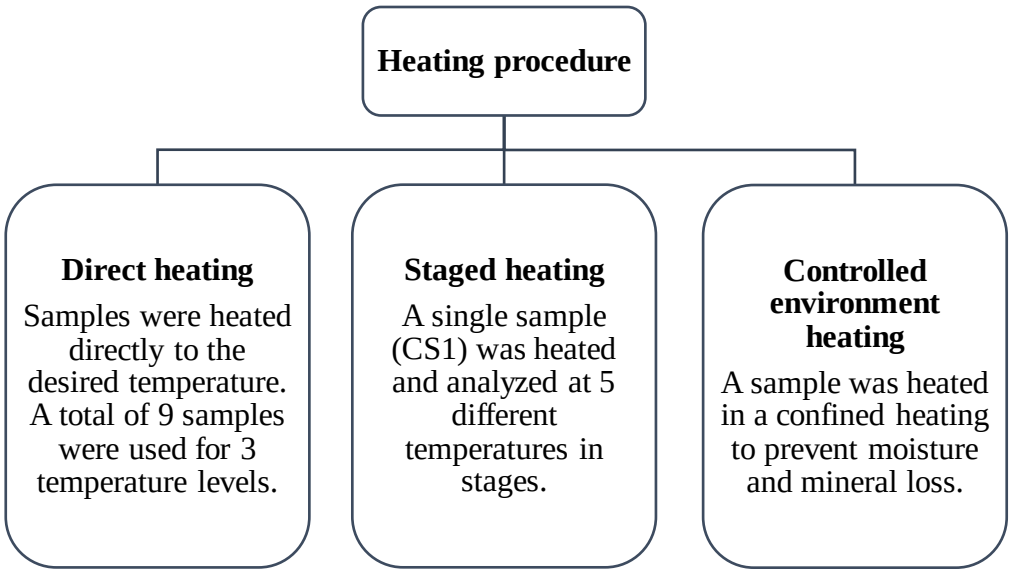

Figure 3.6: Classification of the heating procedure

Table 3.1: Designated temperatures and duration of the direct, staged, and confined heating

Total number of samples	Direct heating (℃)	Staged heating (℃)	Confined heating (℃)	Heating duration (min)
1 (CS1)	N/A	100	N/A	200
3	150	N/A	N/A	250
4 (included CS1)	300	300	N/A	400
1 (CS1)	N/A	400	N/A	500
1 (CS1)	N/A	500	N/A	600
6 (included CS1)	600	600	600	700

One controlled (CS1) sample was selected to examine the difference between direct heating and staged heating on the density and moisture content. Staged heating was performed only on one controlled sample to heat up to 5 different temperatures: 100 °C, 300 °C, 400 °C, 500 °C and 600 °C. The sample was heated to the first desired temperature of 100 °C, and then allowed to cool

down to room temperature before heating it to the new specified temperature. In contrast to staged heating, direct heating was conducted on 9 different samples by heating each 3 samples from room temperature directly to 150, 300 and 600 °C, to see the effect of each temperature individually.

Following to the experimental procedure, the initial heating temperature was set to 20°C. The length of the heating procedure depended on the designated temperature of the experimentation. To ensure the sample is heated uniformly, it was kept at a desired temperature for 2 hours using the specified heat and hold function of the heating equipment. As an example, Figure 3.7 illustrates the heat and hold procedure at 300°C for one sample. As shown in the Figure 3.7, the equipment was heated at a constant rate of 1°C/min to reach the target temperature in 280 mins and was held at that temperature for 2 hours before shutting down. After the samples were cooled down to the room temperature (20°C) naturally, density and moisture content measurements were performed.

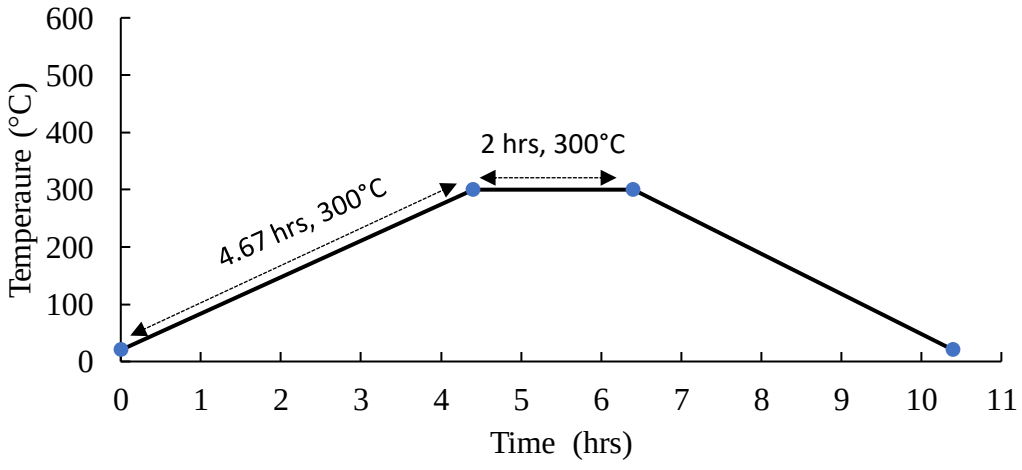

Figure 3.7: Experimental procedure of the direct and staged heating tests

Lastly, in the confined heating test, a special designed hastelloy cell was utilized as shown in Figure 3.8. Hastelloy material was chosen because of its strong oxidation resistance and high temperature strength (Han et. al., 2017). A small particle of the sample was measured and weighed before placing it inside the cell. The cell was closed with the cover, and it was tightened using thread screws to prevent any possible confinement losses. Another particle of the sample was placed on top of the cell in an open environment and both sample parts were heated up to 600 °C. The results from the two sample particles were compared to identify the difference between open versus confined heating.

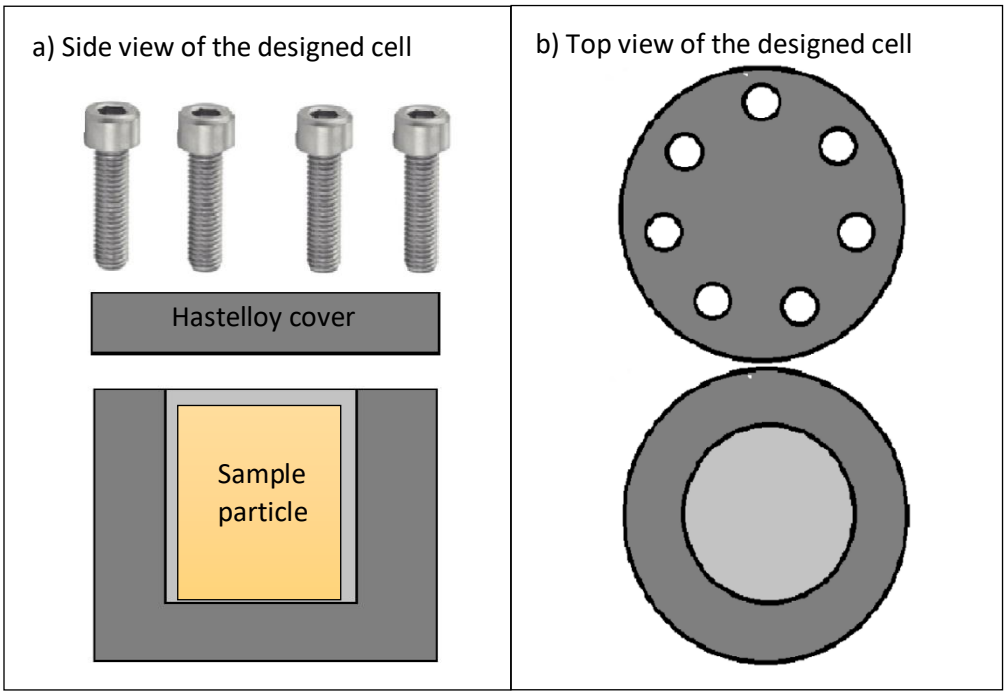

Figure 3.8: Side view and top view of the special designed hastelloy cell

3.4.2 Isotropic consolidation and shearing

Confined triaxial compression test was performed on pre-heated samples at 150℃, 300℃ and 600℃ to assess impact of pre-heating and cooling phase. The rate of cooling phase plays crucial role as pre-heating, since it determines the level of damage through microcracking that would influence post-heated strength. Initially, the consolidation phase was conducted on the samples prior to starting the triaxial testing to achieve at uniform cell pressure alongside the sample inside the cell. This procedure was conducted to simulate the initial in-situ condition of the samples. The reference pressure was set as 2 MPa and each increment was set by 2 MPa within 2 minutes. After each increment, the consolidation stress was held constant for 10 minutes before the next increment. Target consolidation stress was set to 10 MPa before it was lowered to the designated confining pressure (1, 3 and 5 MPa), with the same step procedure as shown in Figure 3.9.

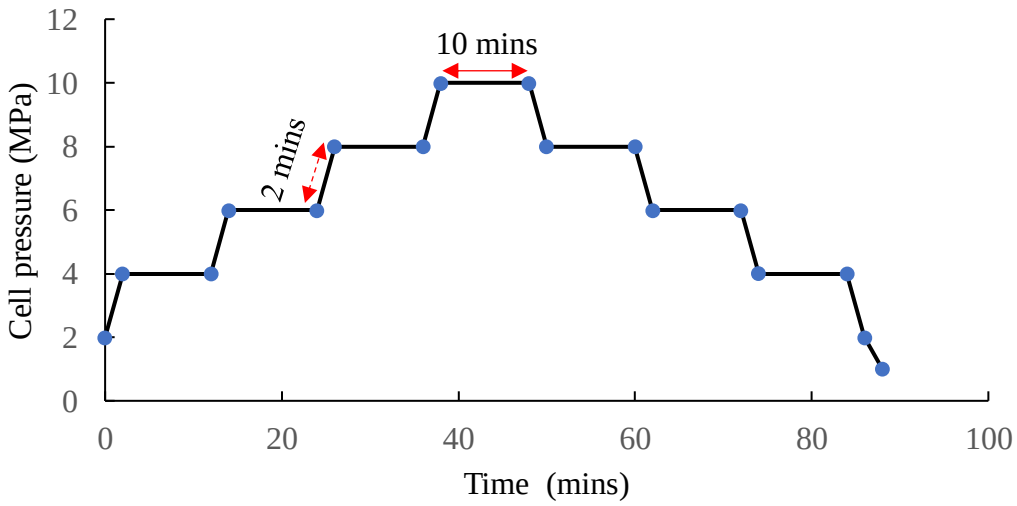

Figure 3.9: In-situ condition re-installation of confined triaxial compression test with 1 MPa

Re-installation phase to initial in-situ condition of the samples was performed by increasing effective confining pressure to specified values to establish similar in-situ conditions and reconstructed with regard to effective stress. Upon completion of the pre-consolidation stage, samples were sheared in a confining triaxial vessel with three different confining pressures (1, 3, 5 MPa) as shown in Table 3.2.

Loading was performed in displacement-controlled mode by implementing vertical load at a rate of 1%/hr and holding the confining radial pressure constant until the failure of specimen.

Table 3.2: Confining triaxial compression testing program

Pre-heated temperature (℃)	**Number of samples**	**Confining pressure (MPa)**
20	1	1
	1	3
	1	5
150	1	1
	1	3
	1	5
300	1	1
	1	3
	1	5
600	1	1
	1	3
	1	5

Chapter 4

4 Results and discussion

4.1 Effect of thermal treatment on physical properties of clay shale

4.1.1 Visual Appearance

Elevated temperatures caused significant changes in color and surface features of tested specimens, as shown in Figure 4.1. The first substantial change in color occurred at 150℃, turning progressively from black to grey as the temperature increased to 300℃. The evaporation of adsorbed and interlayer water, and combustion of organic matter are two of the main reasons for the change that occurred at this stage (Geng and Sun, 2018). At the heating temperature above 300℃, the change in color showed a noticeable shift in colour into a yellowish to brick-red due to the formation of hematite ($Fe_2O_{3)}$ under oxidizing conditions (Sun et al., 2016).

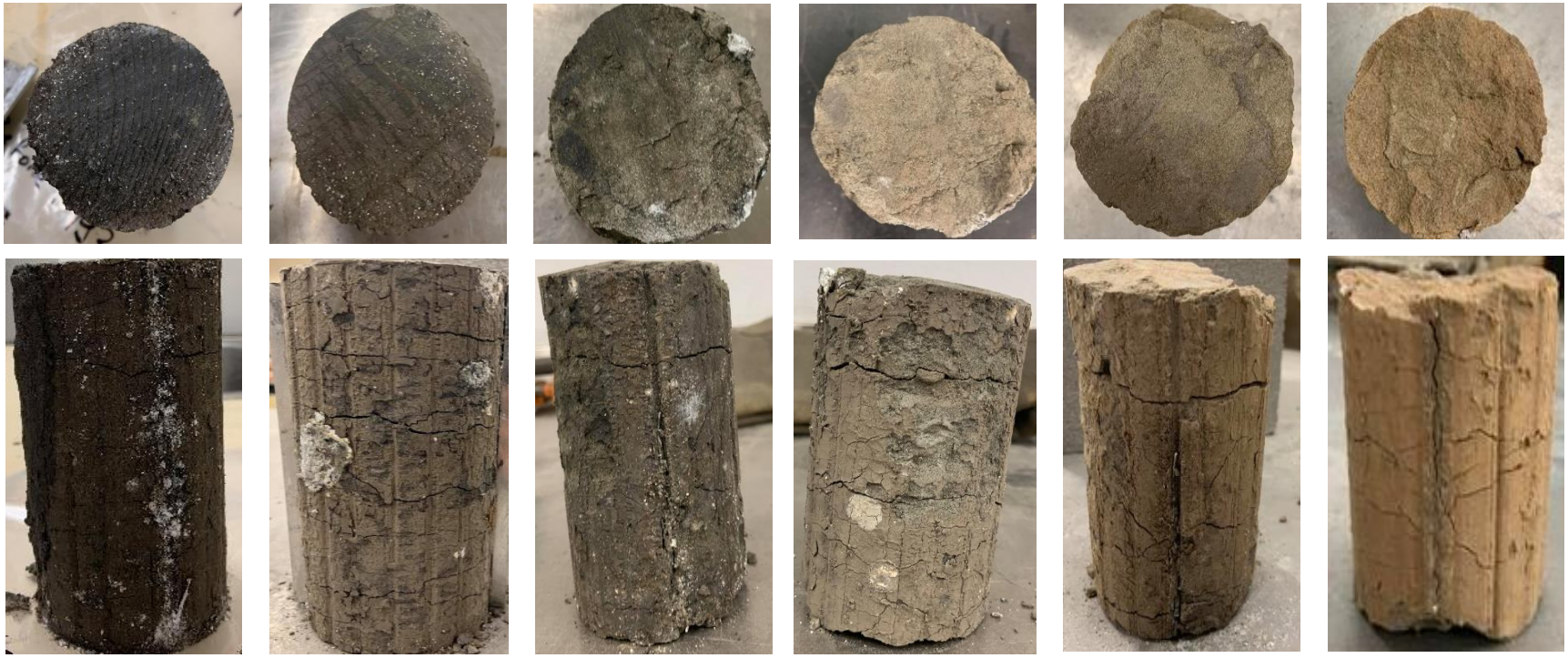

Figure 4.1: Change in colors and shapes of clay shale specimens at high temperature treatments

To examine if the color change during heating of the sample is due to the oxidization of organic material in clay, the hastelloy cell was used. A sample particle was placed inside the sealed hastelloy cell to prevent iron oxidation and to create confined heating. Another sample particle was placed on top of the cell in an open environment to compare the difference between the two conditions. Both sample particles were heated up to 600 °C with a rate of 1 °C/min. Figure 4.2 illustrates a comparison of the experiment results conducted under two different conditions. As revealed by this figure, the sample particle inside the sealed cell did not have a significant color change, while the surface appearance of the heated sample under the open environment heating test turned into yellowish to brick-red.

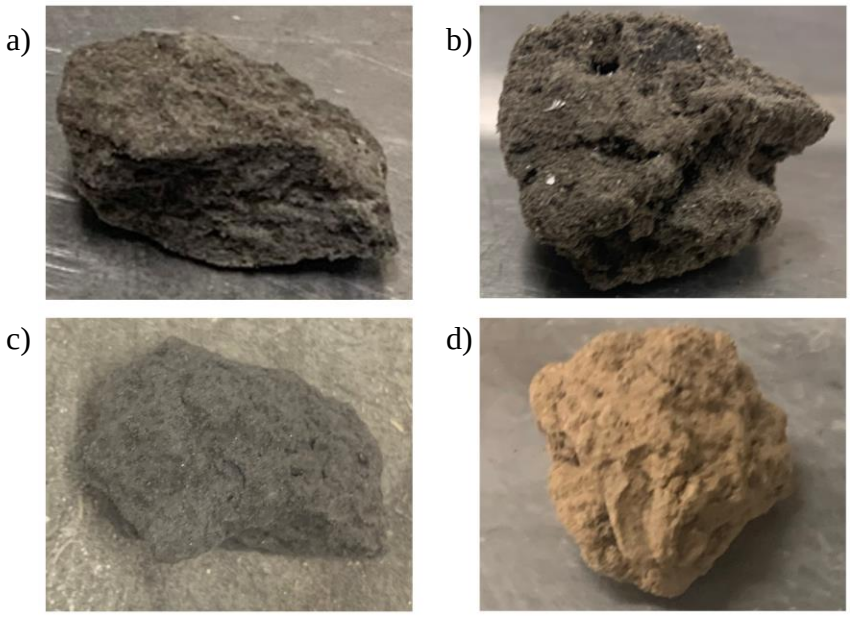

Figure 4.2: Comparison of open and confined effect on mineralogy and texture of clay shale, where: a) before heating in confined environment; b) before heating in an open environment; c) after heating in confined environment; d) after heating in open environment

During the heating test at different temperatures, cracks start to develop on the surface of the clay. The formation of cracks and color change are found to be associated with the chemical and physical changes of the sample after exposure to high temperatures. In addition, cooling phase is critical for the crack formation and structure after completion of heating. This could be a major reason for having different rate of cracking on every sample. The vertical and horizontal crack formation rates of the samples with temperature were calculated using the below:

$$CFR = \left(\frac{N_f}{N_i} - 1\right) \times 100\% \quad (1)$$

where CFR is the crack formation rate (%), N_i and N_f are initial and final number of cracks on surface of the sample, respectively. The initial and final number of the cracks were identified by visual observation of the same surface before and after heating experiment as shown in Figure 4.3. Moreover, it is observed that when the temperature is less than 300℃, minor visual cracks start to appear on the surface, as shown in Figure 4.2. As the temperature increases above 300℃, the number of cracks and crack apertures gradually increase accompanied by forming the horizontal crack network.

Figure 4.3: Crack identification of the sample before and after heating treatment

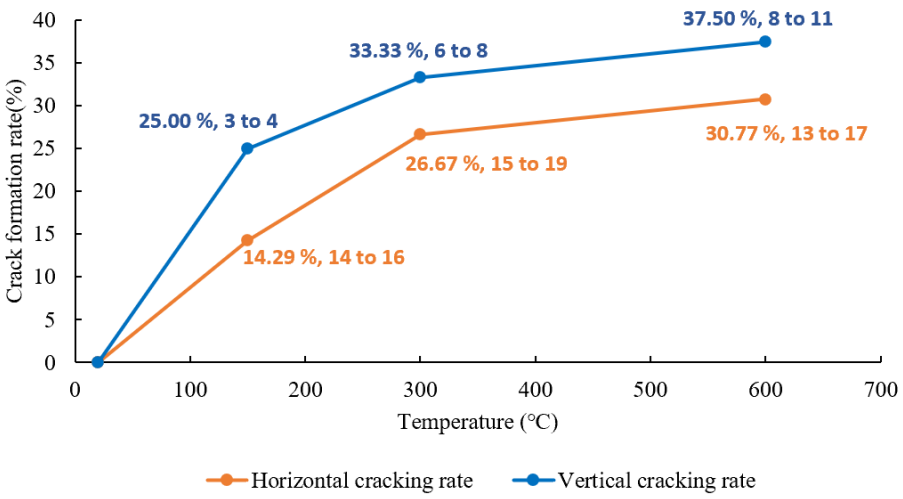

Figure 4.4: Horizontal and vertical cracking formation rate with increasing pre-heated temperature

4.1.2 Weight loss and density

Weight loss is hereby defined as the ratio of a specimen's weight loss after thermal treatment to its original weight:

$$\zeta = \left(\frac{m_1 - m_2}{m_1}\right) \times 100\% \qquad (2)$$

where ζ is mass loss rate (%), m_1, m_2 are masses of a specimen before and after thermal treatment, respectively. Bulk density of a specimen can be obtained using the mass and volume of sample.

Figure 4.5 shows bulk density variations and weight loss at high treatment temperatures of a controlled sample CS1 during staged heating. It is observed that both parameters of a clay shale are affected substantially by the temperature. Hence, to analyze them, obtained results are divided into three phases: room temperature to 100℃, 100℃ to 300℃ and above 300℃.

Minor changes in weight and density were recorded at the first stage. This minor change was due to the vaporization of adsorbed and interlayer water (Sun et al., 2016). A significant amount of reduction in weight and bulk density occurred during the second phase. The reduction in weight at this phase was found to be 15.5% which accounts for 89% of the total mass loss, while the bulk density reduced from 2.29 g/cm^3 to 1.94 g/cm^3, which accounts for 6.9%. The main reason for such a high reduction of weight and density could be due to the evaporation of absorbed and interlayer waters (Guo et al., 2020; Sun et al., 2016).

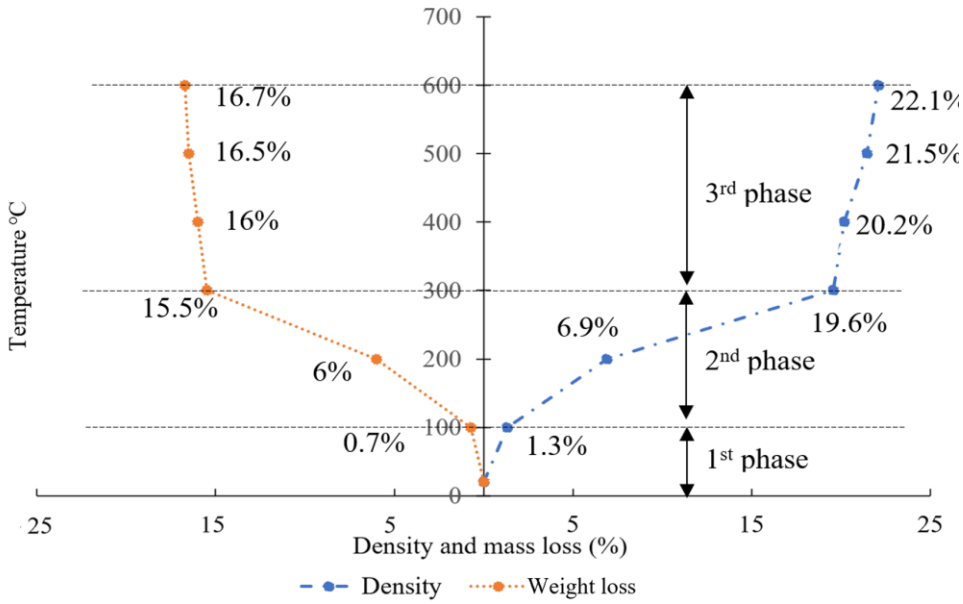

Figure 4.5: Change in density and weight loss at varying temperatures

During the third phase, as the temperature rises above 300℃, increase in weight loss and bulk density reduction continued at a slower pace. Presumably, at the temperature range of the third phase changes are dominated by dissipation of structural water and decomposition and oxidation of organic matter (Han et al., 2017).

Moreover, further experiments were conducted to compare the weight loss and bulk density reduction differences between staged and direct heating (Figure 4.6 and Table 4.1). It can be observed that the change in weight loss follows a similar trend to the crack formation rate, as shown in the figure.

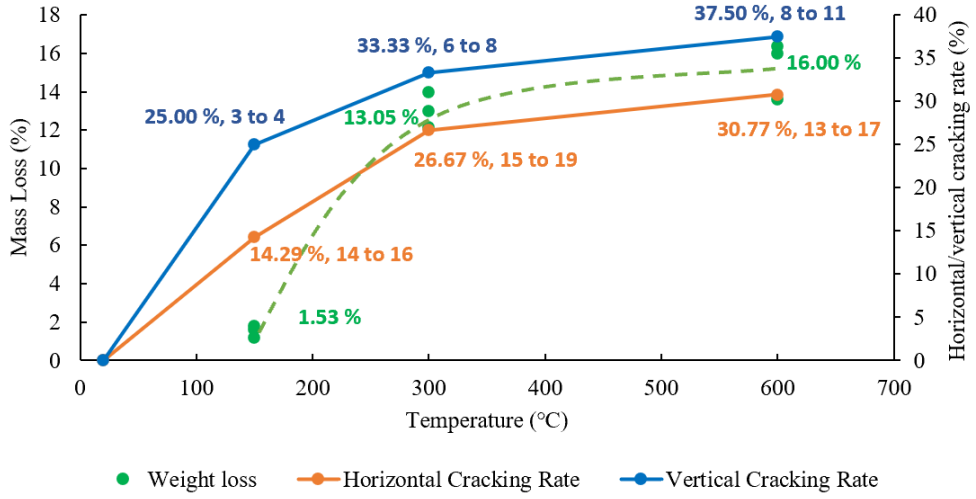

Figure 4.6: Percentage weight loss and cracking formation rate of nine samples during direct heating at 150℃, 300℃ and 600℃

A total of nine samples were heated from room temperature directly to 150℃, 300℃ and 600℃ (Figure 4.6) during the direct heating stage. Results show similar trends with the staged heating where mass loss increases with the increment of temperature. An average of 1.53% weight loss was recorded at 150°C, while it increased significantly to 13.05% when the temperature was raised to 300°C. Similar to staged heating, minor change in weight loss was recorded under direct heating at the temperature above 300°C.

Initial and final density measurements of directly heated clay shale samples were summarized in Table 4.1. Obtained data shows that the density drops with

increasing temperature, and the higher temperatures have significant density drops compared to low temperatures, which agrees with the results of staged heating.

Table 4.1: Effect of temperature on bulk density during direct heating

Temperature (°C)	Bulk density at 20°C (g/cm^3)	Bulk density After (g/cm^3)	Bulk density loss (%)
150	1,986	1,962	1.21
	1,631	1,606	1.53
	1,884	1,851	1.75
300	1,991	1,734	12.91
	1,956	1,719	12.12
	1,933	1,680	13.09
600	1,969	1,715	12.90
	2,514	2,054	18.30
	1,940	1,623	16.34

4.1.3 Mineral transformation

The mineralogical composition of clay shale was obtained through X-Ray diffraction testing. Results of bulk minerals content at treatment temperatures of 20°C, 300°C and 600°C showed that quartz was the main component, as illustrated in Figure 4.7. A significant drop in the peak intensity of quartz was observed when increasing the heating temperature from 20°C to 300°C while no significant changes in the peak intensity of quartz were recorded from 300°C to 600°C. Moreover, XRF analysis showed that oxides that existed in clay including Na_2O, MgO, Al_2O_3, SiO_2, Fe_2O_3 and other oxides in minor amounts (Table 4.2). Based on this table, the color change of the sample to initially darker colors is related to the combustion of organic material. However, further color change to yellowish to

brick-red color is due to the formation of hematite (Fe_2O_3) as heating took place in oxidizing environment. Similar color changes were also observed by Geng and Sun (2018).

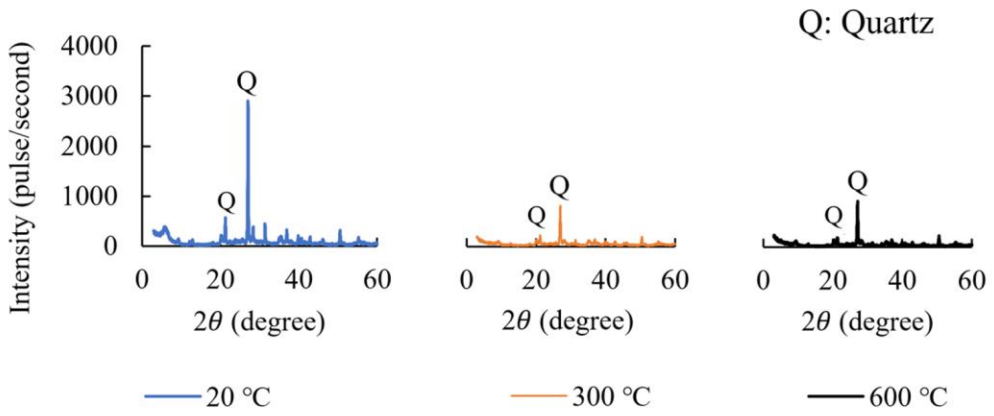

Figure 4.7: Bulk mineral content at different treatment temperatures

Table 4.2: Chemical composition (mass percentage) of clay sample at different treatment temperatures

T (°C)	Na_2O	MgO	Al_2O_3	SiO_2	P_2O_5	SO_3	K_2O	CaO	TiO_2	Fe_2O_3	SrO
20	0.27	3.01	18.10	62.06	0.07	1.60	3.45	2.00	1.04	8.40	0.07
300	0.53	3.81	22.06	74.56	0.11	1.98	3.79	2.37	1.05	8.02	0.06
600	0.44	3.74	22.47	75.59	0.10	1.90	3.82	2.14	1.08	8.42	0.06

Other than the bulk mineral composition of the sample, Figure 4.8 illustrates clay mineral content within the sample at treatment temperatures between 300°C-600°C. Substantial changes in mineralogy were not detected other than slight decrement of kaolinite from 84% to 74% and increment of illite from 13% to 19%. This could be because of dehydration of kaolinite and decomposition of illite. In

case of kaolinite, it dehydrates because the outer layer of kaolinite gets removed at 470℃-520℃ and the inner layer of kaolinite gets removed at 540℃ (Han et al., 2017; Fontaine et al., 2018). These types of reactions will transform kaolinite into highly reactive amorphous material at 600℃. The dehydration and then dihydroxylation of kaolinite is provided below:

$$Al_2O_3 \cdot 2SiO_2 \cdot 2H_2O \xrightarrow{470-520℃} Al_2O_3 \cdot 2SiO_2 \cdot \frac{1}{2}H_2O + \frac{3}{2}H_2O \quad (1)$$

$$Al_2O_3 \cdot 2SiO_2 \cdot \frac{1}{2}H_2O \xrightarrow{>540℃} Al_2O_3 \cdot 2SiO_2 + \frac{1}{2}H_2O \quad (2)$$

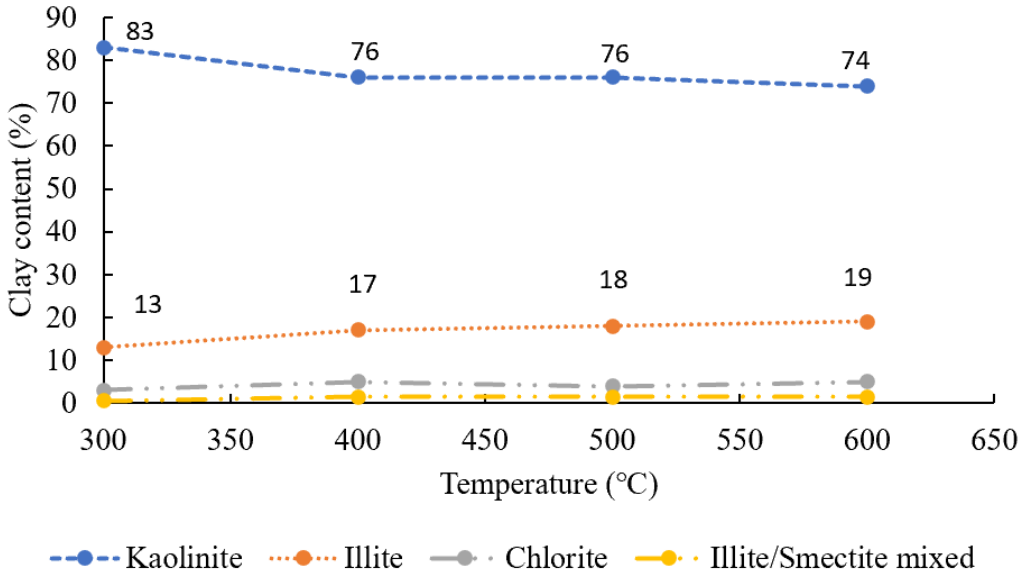

Figure 4.8: Clay content at different treatment temperatures

Further experiments were conducted using XRD and XRF to analyze the difference between open and confined heating on mineralogical changes with temperature. Two powdered samples were prepared and tested in both types of equipment before heating to determine the initial mineralogical composition. After conducting open and confined heating experiments, the powders were tested again

using XRD and XRF equipment. The results are illustrated in Table 4.3 and Figure 4.9.

Table 4.3: Elemental composition of clay shale powder at open and confined heating environments (%)

Condition	ZrO_2	MgO	Al_2O_3	SiO_2	P_2O_5	SO_3	K_2O	CaO	TiO_2	Fe_2O_3	SrO
Before	0.07	3.32	15.07	66.52	0.07	0.63	3.58	4.45	0.98	**5.28**	0.03
Confined heating	0.05	3.46	**15.27**	**66.85**	0.10	**0.73**	3.21	4.39	0.74	**5.19**	0.03
Open heating	0.05	3.43	**15.14**	**66.65**	0.09	**0.69**	3.22	4.49	0.74	**5.47**	0.03

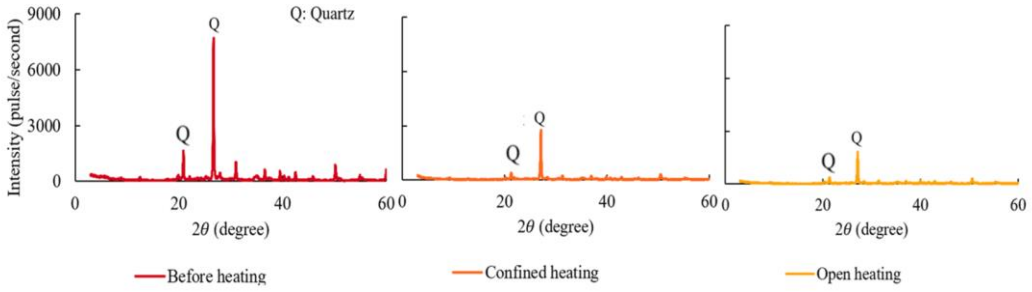

Figure 4.9: Bulk mineral content of samples tested in open and confined heating environments before and after experiment

4.2 Effects of thermal treatment on mechanical properties of clay shale

4.2.1 Stress-strain and volume change behavior

The stress-strain and volume change behavior of Wabiskaw formation clay shale under confined triaxial compression test (TC) at various temperatures and confining pressures are presented in Figures 4.10–4.16 and Figures A.1-A.4.

Initially, all specimens showed densifying and hardening behavior during compression due to the closure of pre-existing microcracks and bedding plane gaps.

Post-peak deviatoric stress dropped abruptly with increasing axial strain. This sudden drop is related to the change in crack occurrence and deformation in the sample. Post peak deformation is mainly dominated by translation movement of the specimen's two portions following their slide, as shown in Figure A.7-A.8. The post-peak compression continued to achieve the ultimate (post-peak) condition where deviatoric stress became constant.

From Figures 4.10-4.12, it can be observed that deviatoric stress increased with increasing temperature due to the hardening of samples by thermal pre-treatment. Moreover, for all three confining pressures, at higher temperatures, the pre-peak path is stiffer compared to the lower temperatures.

Furthermore, for some triaxial compression curves, maximum deviatoric stress is obtained at higher axial strains as the confining pressure and temperature increase. As an example, for 1 MPa confining pressure (Figure 4.10) and treatment temperatures of 150℃ and 600℃, maximum deviatoric stress was acquired at the axial strain of 2%. Whereas, at confining pressure of 3 MPa (Figure 4.11), for the same temperatures, the axial strain has increased within the range of 3.5 – 5.5%. This is due to the tendency of the specimen to accommodate higher axial strain before failure due to confinement. In other words, as the confining pressure and temperature increase, rock's potential for post-peak (ultimate) fracture decreases. This further confirms that the sample becomes stiffer and brittle with increased temperature. This phenomenon could be seen at confining pressures of 1 MPa and 3 MPa (Figures 4.10-4.11) where constant deviatoric stress is achieved at the axial strain of 3% and < 6%, respectively. In addition, it was observed that deviatoric

stress for 150℃ at 3 and 5 MPa was lower compared to 20℃ at corresponding confining pressure. This was due to the weak microstructure and macrostructure of the sample used in this experiment, as shown in Figure A.9.

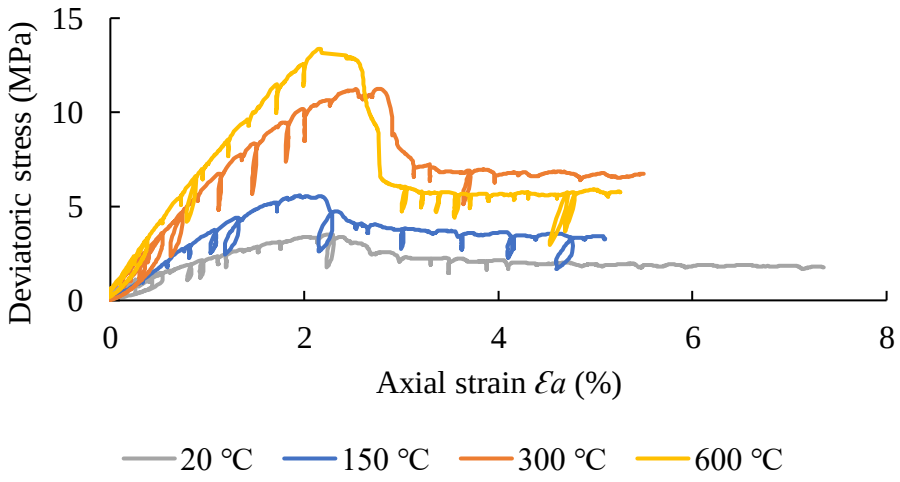

Figure 4.10: Deviatoric stress vs axial strain at various temperatures under confining pressure of 1 MPa

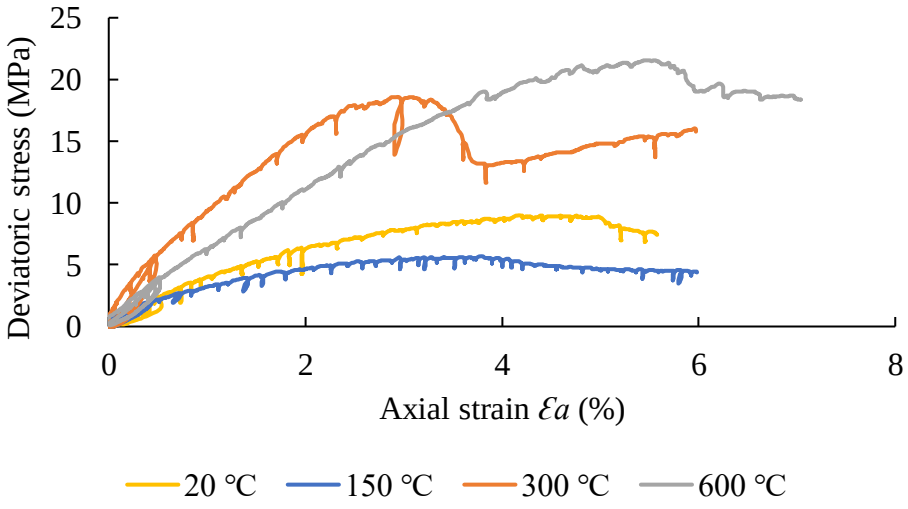

Figure 4.11: Deviatoric stress vs axial strain at various temperatures under confining pressure of 3 MPa

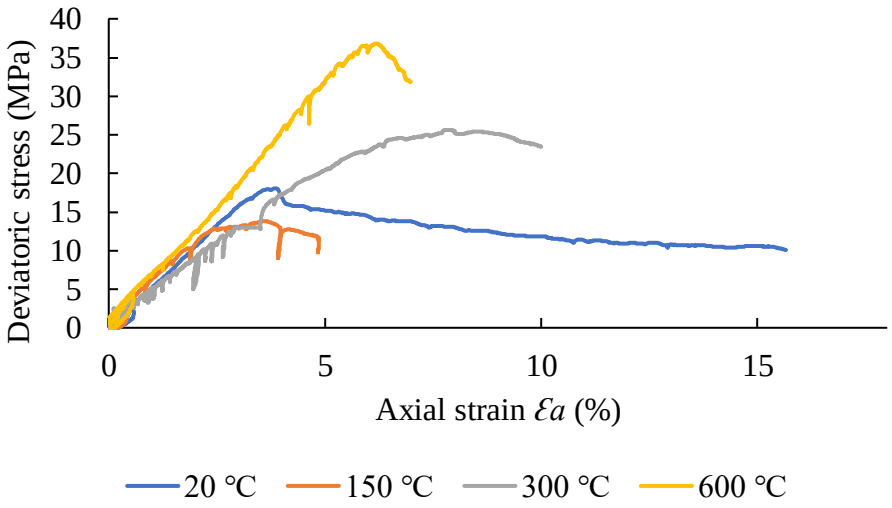

Figure 4.12: Deviatoric stress vs axial strain at various temperatures under confining pressure of 5 MPa

Figures 4.13-4.16 show the relationship between deviatoric stress, principal stress ratio, volumetric strain (ε_v) and axial strain (ε_a) for tested temperatures and confining pressures. In addition, the obtained slope (m) from the volumetric strain and axial strain plot is illustrated in Table 4.3. Based on these figures, samples fail due to dilation at lower confining pressure, while shear failure is more dominant at higher confining pressures. It is due to increased confining pressure providing a higher allowance for the compression of the sample before dilation. Moreover, slope data obtained via volumetric strain and axial strain relationship proved that at 1 MPa, the failure was mainly due to the dilation when the slope had a positive value. In contrast, the negative values occurred at 3 MPa and 5 MPa in the slope indicated that the failure was mainly due to the compression. There was an exception in the sample at 300℃ under 3 MPa, where the slope was showing failure

was occurred due to the dilation. This could be due to the physical parameters of the specific sample that was tested under this condition.

Table 4.3: Slope obtained by volumetric strain (ε_v) and axial strain (ε_a) relationship

Temperature (℃)	1 MPa	3 MPa	5 MPa
20	+0.19	N/A	-0.35
150	-0.04	-0.25	-0.71
300	+0.22	+0.55	-0.42
600	-0.05	-0.74	-0.44

For this study, the specimens were assumed to fail at maximum deviatoric stress. This is due to the occurrence of cracks and deformation caused by pre-heat treatment post-peak deviatoric stress. The dilative failure of the samples at lower confinement was identified based on the positive slope of volumetric strain vs axial strain at peak deviatoric stress. Further, with the increased confinement pressure, the volumetric strain slope indicated shear compression failure.

Also, it is necessary to note that samples that were pre-heated at lower temperatures showed the highest volumetric strain. Further, this confirms the more ductile state of samples at low temperatures and the brittleness of the heated rock samples.

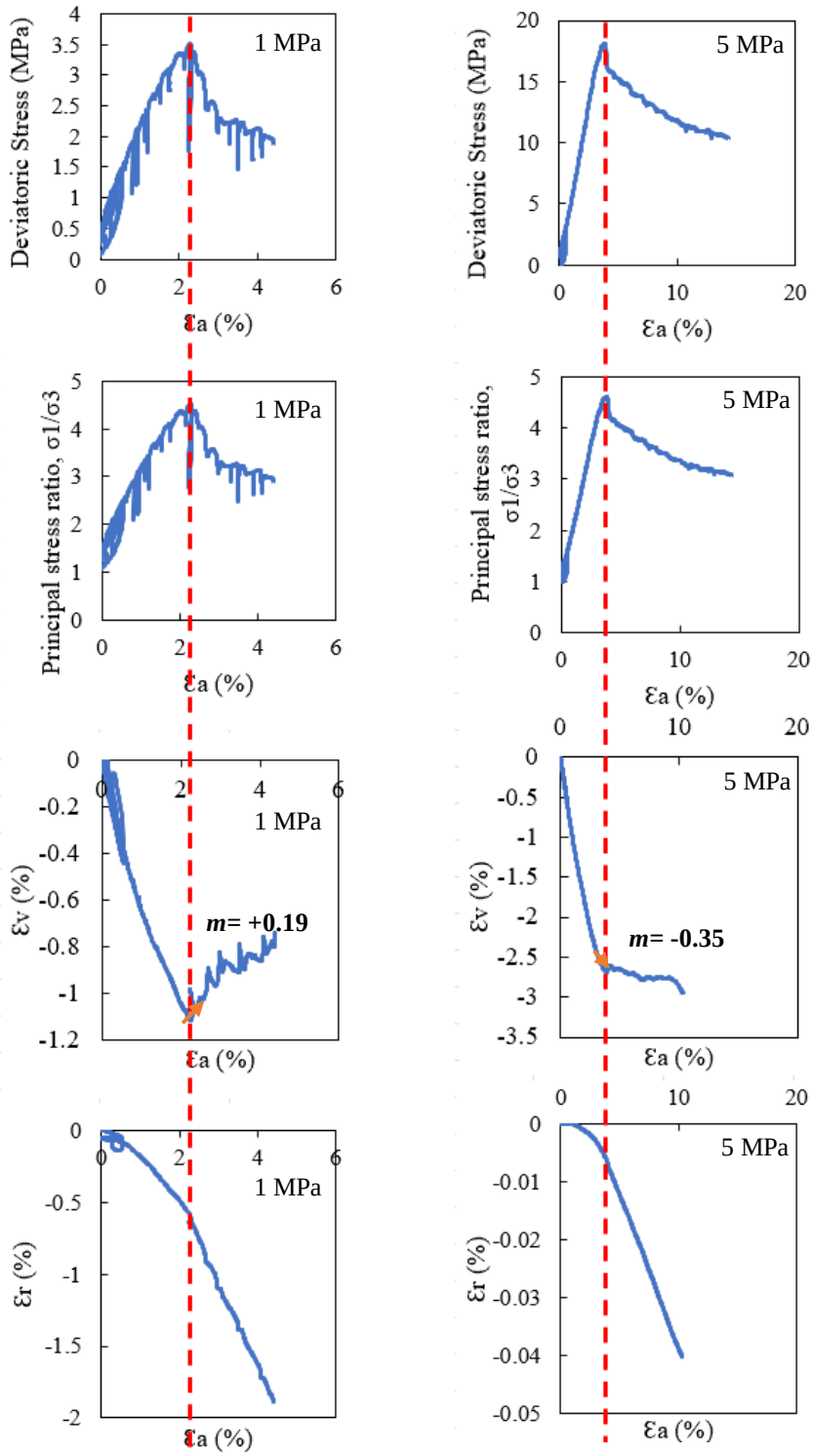

Figure 4.13: Stress-strain curves at 20°C under confining pressures of 1 MPa and 5 MPa

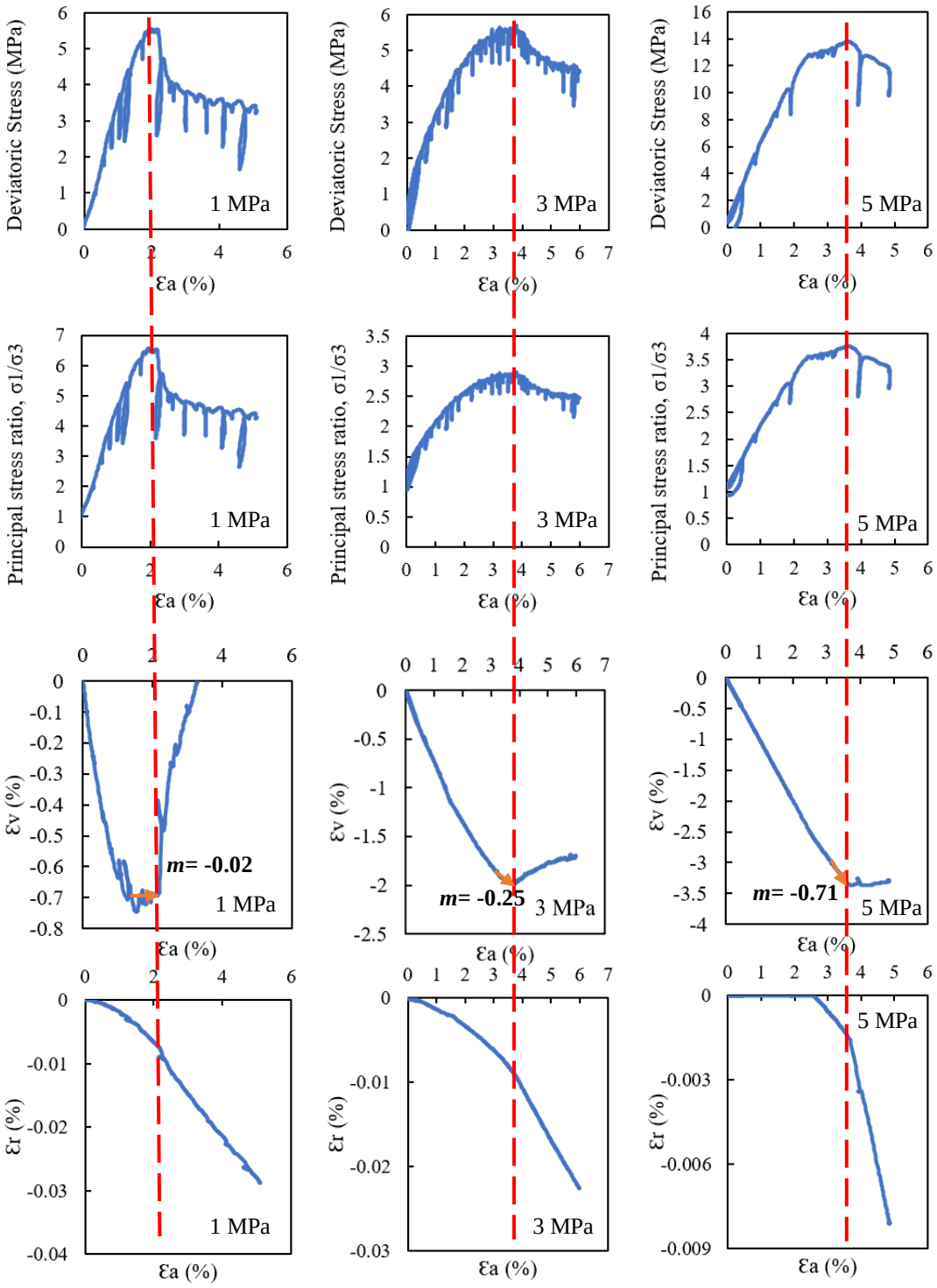

Figure 4.14: Stress-strain curves at 150°C under confining pressures of 1 MPa, 3 MPa and 5 MPa

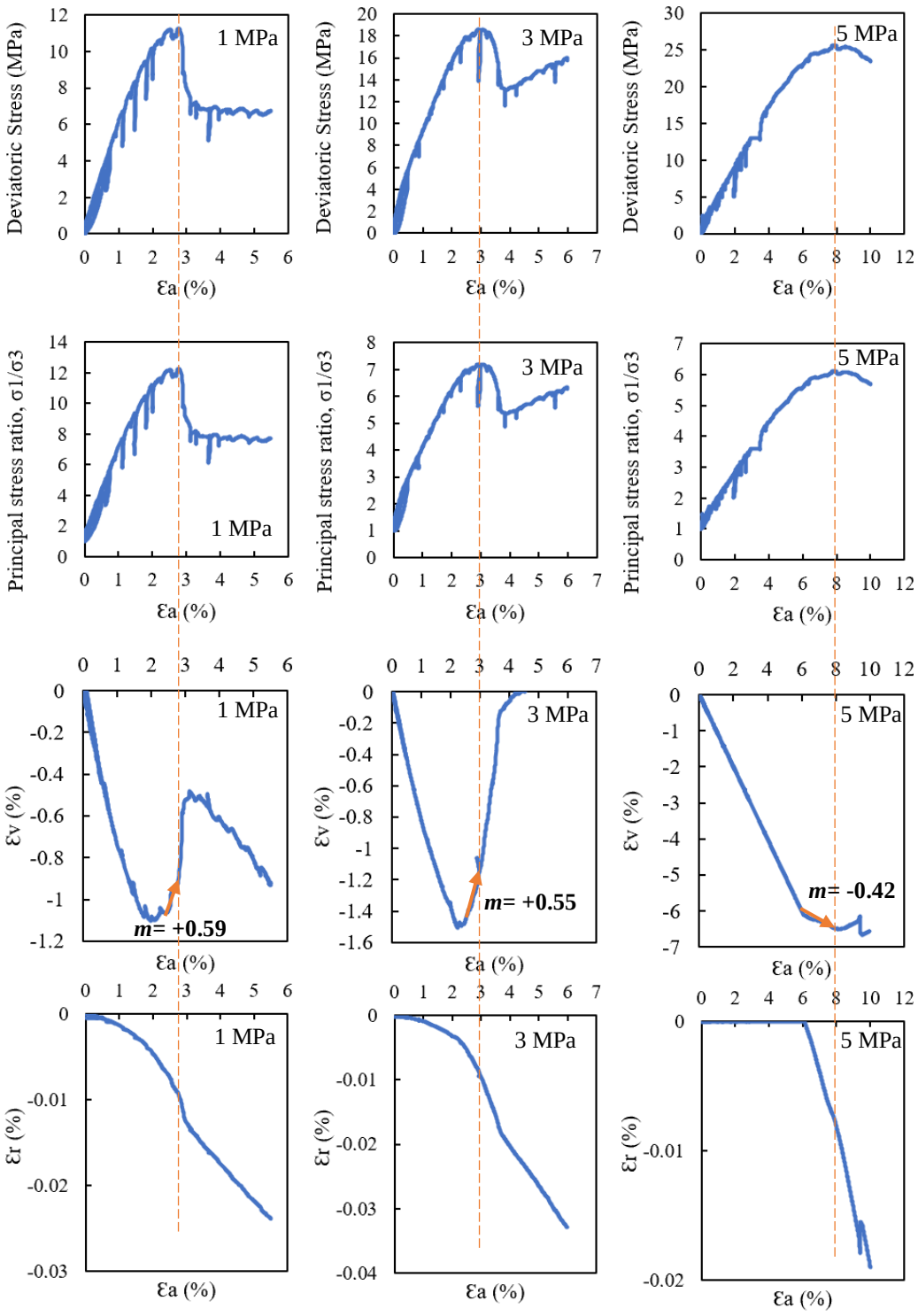

Figure 4.15: Stress-strain curves at 300°C under confining pressures of 1 MPa, 3 MPa and 5 MPa

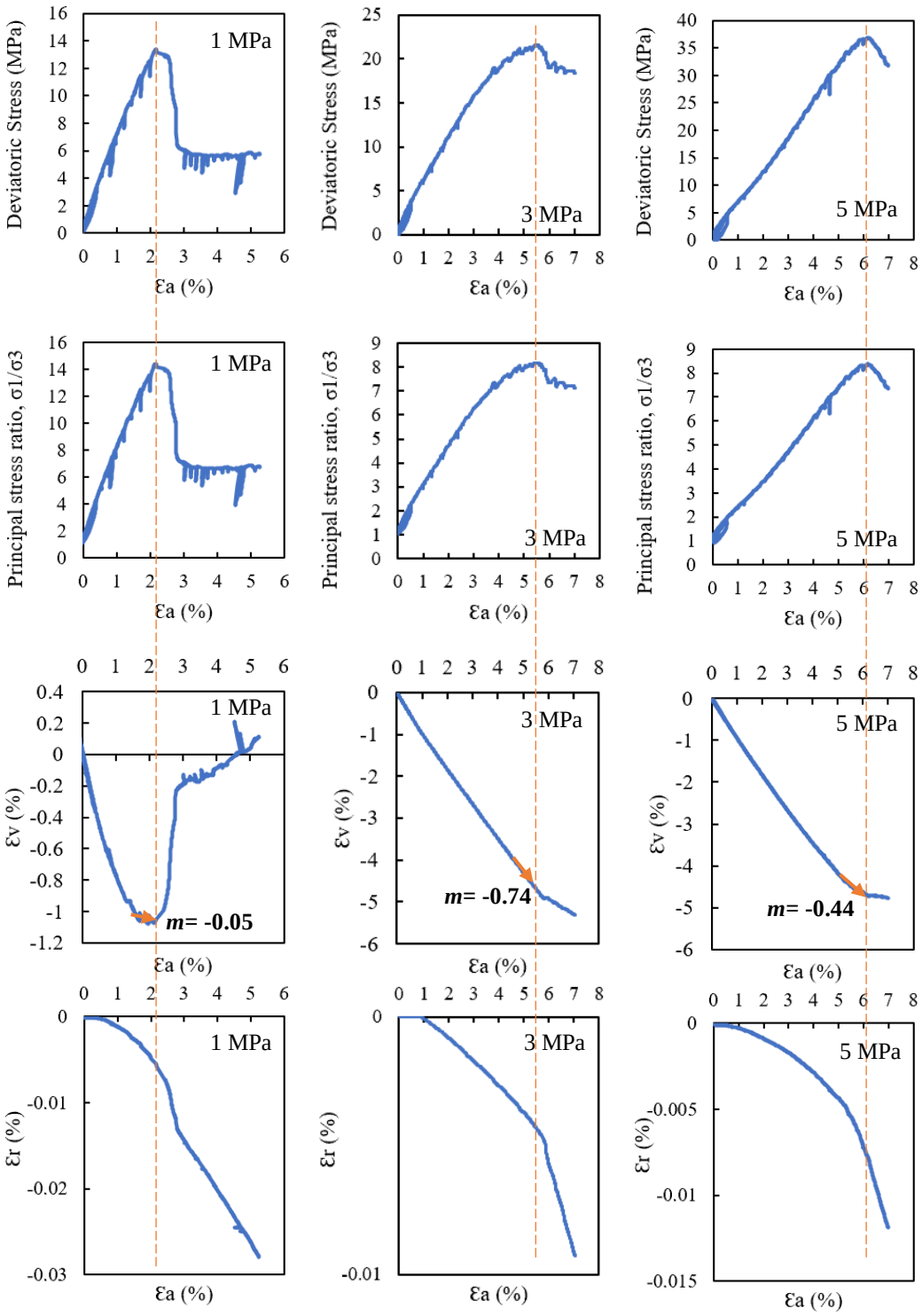

Figure 4.16: Stress-strain curves at 600°C under confining pressures of 1 MPa, 3 MPa and 5 MPa

Figure 4.17 illustrates the relationship between the peak principal stress ratio and the confining pressure. At 20℃, the stress ratio had an almost linear trend at $\sigma1/\sigma3$ = 4.5 regardless of the confining pressure. However, the increasing temperature peak principal stress ratio decreases with increasing confining pressure. Also, it is depicted from Figure A.6 that increasing temperature increased the peak principal stress ratio while increasing confining pressure had an opposite effect. The exception occurred at 150℃ due to the weak microstructure and macrostructure after conducting pre-heating treatment as shown in Figure A.9.

Similar results were illustrated using the relationship between deviatoric stress and the confining pressure; relationship between maximum principal stress and confining pressure is in Figures A.5-A.6.

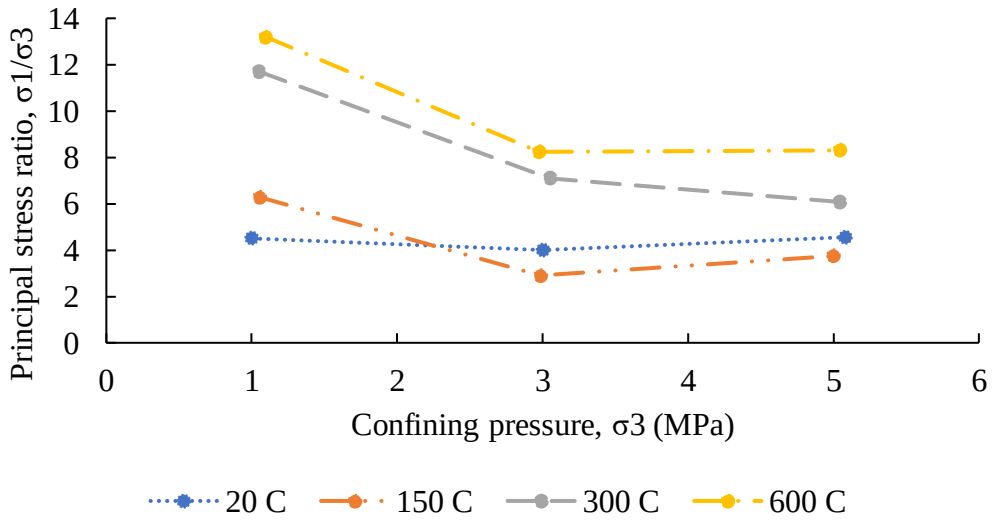

Figure 4.17: Peak principal stress ratio vs confining pressure at 20℃, 150℃, 300℃ and 600℃

4.2.2 Elastic response

The confined triaxial compression test was used to identify the elastic response of clay shale samples. Poisson's ratio and deformation modulus were determined using the initial linear response region on stress-strain graphs.

The change of deformation modulus with temperature is shown in Figure 4.18. Overall, the deformation modulus increased with the temperature for all confining pressures. The elastic modulus of the granular materials mainly depends on the compositional phases and the boundaries between those phases. Further, it is typical for the moisture content to be in equilibrium with air humidity (Húlan et al., 2015; Trnik et al., 2011). During the heating of the samples, the dehydration process takes place, making the connection between clay lattice structures. This then leads to an increment of the elastic modulus of the sample. Therefore, the elastic properties of the samples are primarily affected by the amount of water between the surfaces and not the compressibility of water.

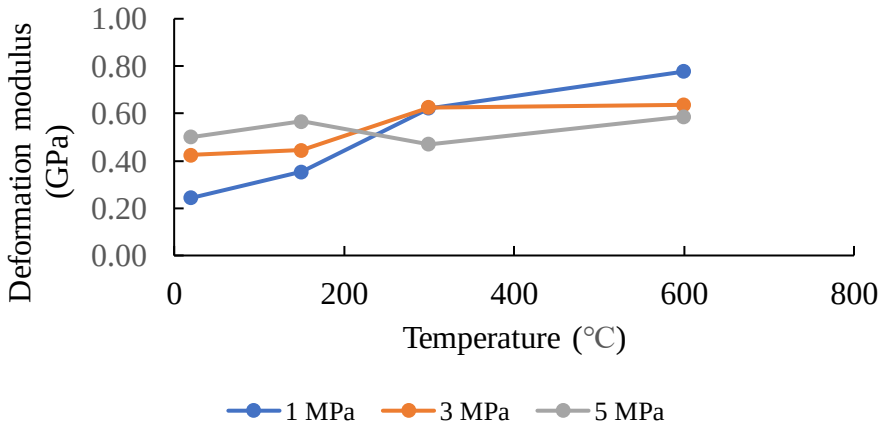

Figure 4.18: Deformation modulus vs treatment temperature (20°C, 150°C, 300°C and 600°C) at confining pressures of 1 MPa, 3 MPa and 5MPa

The effect of the confining pressure on deformation modulus is shown in Figure 4.19. Deformation modulus increased with confining pressure at the temperatures of 20℃ and 150℃.

Additionally, the deformation modulus at 20℃ showed a higher increment compared to 150℃ for the same confinement pressures. This could be due to an increment in stiffness for samples at room temperature coming solely from confining stress. This could be due to an increment in stiffness for samples at room temperature coming solely from confining stress.

In contrast to lower temperatures, deformation modulus decreased with increasing confining pressure at the temperatures 300℃ and 600℃. This might be due to the increased brittleness of the samples. As the samples were heated to higher temperatures, they became more brittle with a higher density of micro-cracks. After, as the loads were applied to the samples failed at lower loads.

Further, it can be noted that the deformation modulus attempts to reach a constant value of 0.55 GPa with increasing confining pressure. This might be due to the lesser effect of fractures and pore fluids at higher confinement pressure.

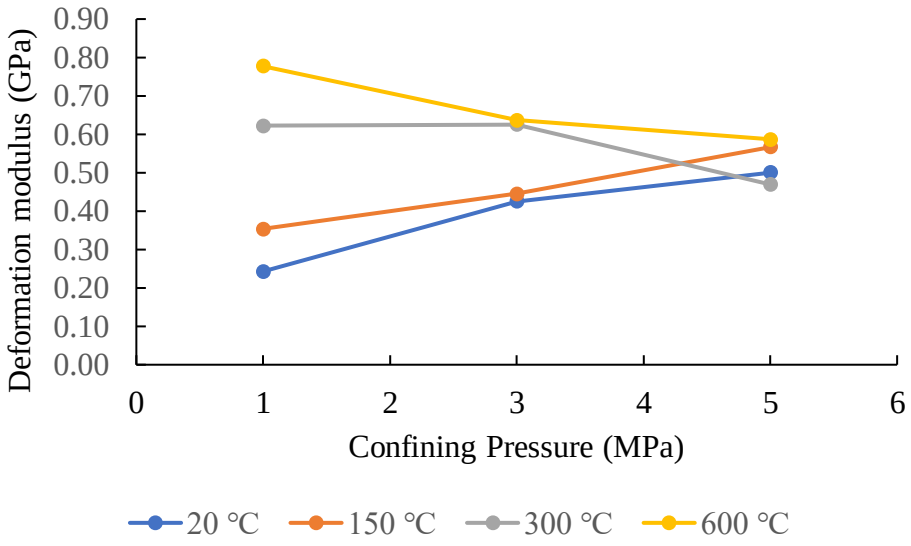

Figure 4.19: Deformation modulus vs confining pressure (1 MPa, 3 MPa and 5MPa) at treatment temperatures of 20℃, 150℃, 300℃ and 600℃

The evolution of Poisson's ratio as a function of four treatment temperatures (20℃, 150℃, 300℃ and 600℃) and three confining pressures (1 MPa, 3 MPa and 5 MPa) are shown in Figures 4.20 – 4.21. Poisson's ratio decreased with increasing temperature and confining pressure. This also confirmed that samples became more brittle with heat treatment.

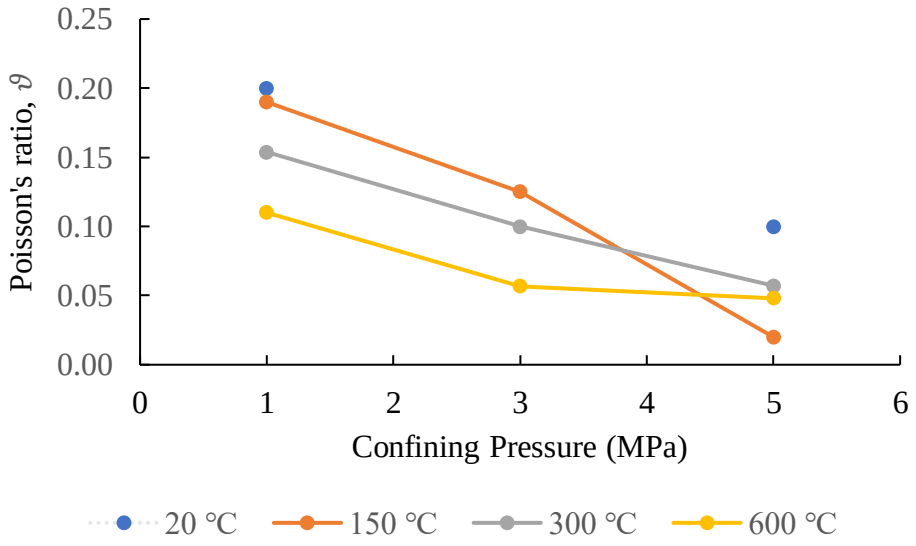

Figure 4.20: Poisson's ratio vs confining Pressure (1 MPa, 3 MPa and 5MPa) at treatment temperatures of 20℃, 150℃, 300℃ and 600℃

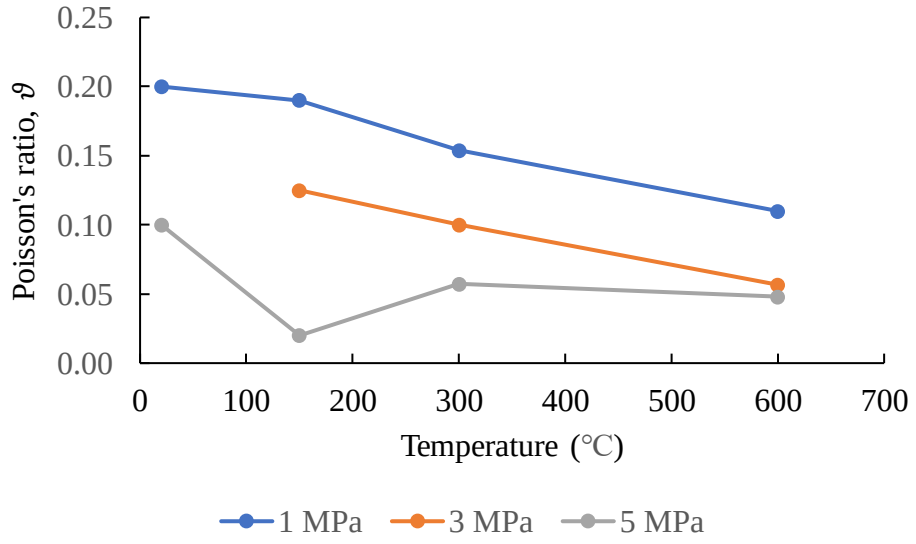

Figure 4.21: Poisson's ratio vs treatment temperature (20℃, 150℃, 300℃ and 600℃) at confining pressures of 1 MPa, 3 MPa and 5MPa

4.2.3 Peak strength response

Peak strength is the maximum value of deviatoric stress in a stress-strain curve obtained from conventional triaxial compression tests. Corresponding values of peak strength and treatment temperature under three confining stresses of 1 MPa, 3 MPa and 5 MPa are illustrated in Figure 4.22. It can be observed that the distribution of peak strength values is somehow scattered and non-linear at lower treatment temperatures which has also been noticed in previous studies Tian et al. (2014) while studying claystone from Auguste – Victoria hard coal mine. This phenomenon could be due to the variations in mineralogy, moisture content, amount and distribution of pre-existing microcracks, as well as microstructures of different samples used during the experiments. Nonetheless, after treatment temperatures of 300℃ and 600℃, the peak strengths of specimens are 2 to 2.5 times greater in comparison with the room temperature. The total rate of q is higher until the heating temperature of 300℃, following lower steadier rates up to 600℃. Evaporation of water, closure of existing microcracks and crystallization of clay minerals could be the main reasons for high incremental rates at lower temperatures (before 300℃). In addition, the results obtained shows that below 300℃, clay shale rock's density increases faster following almost constant values, making rocks denser and stronger. On the other hand, gradual slowing down of peak stress in the range of 300℃ - 600℃ could result from thermal cracks. Thermal cracks weaken the effects of crystallization and closure of microcracks to some extent, preventing further significant improvements of peak stress.

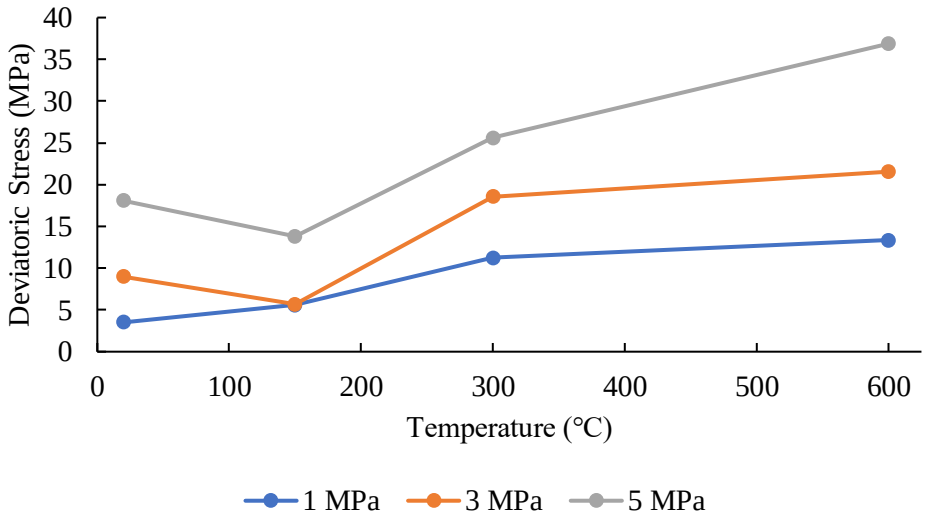

Figure 4.22: Peak strength vs temperature as a function of three confining pressures

The peak strengths of clay shales are strongly influenced by confining pressures. As can be seen from Figure 4.22 greater the confining pressure, greater the compressive strength of the material for almost all treatment temperatures. Effects of confining pressures were observed to be the lowest during the heating temperature of 150°C, where no changes in axial stress were observed as confining stress increased from 1 MPa to 3 MPa. Furthermore, for the same treatment temperature, increment of confinement stress from 1 MPa to 5 MPa also produced the smallest gain in axial stress of 8 MPa, compared to 600°C, where it resulted in the highest gain of 24 MPa for the same range of confining pressures.

Another useful graphical technique to determine the strength properties of clay shale samples is by plotting Mohr circles or failure envelope with the data from the triaxial compression test. Mohr circles are drawn for maximum axial stress (at

failure) and confining pressures (cell pressure) for all 12 specimens tested. Figures 4.20-4.23 show Failure envelopes of tested samples at four treatment temperatures (20℃, 150℃, 300℃ and 600℃) under confining pressures of 1 MPa, 3 MPa and 5 MPa. Corresponding values of cohesion *c* and angle of shearing resistance ϕ (friction angle) obtained from the graphs are shown in Table 4.4.

Table 4.4: Experimentally obtained values of cohesion, and friction angle at treatment temperatures of 20℃, 150℃, 300℃ and 600℃.

Temperature (℃)	**Confining Pressure (MPa)**	**Cohesion, *c* (MPa)**	**Angle of friction, ϕ (Deg)**
20	1,3,5	0,01	39,43
150	1,3,5	1	30
300	1,3,5	2	39,09
600	1,3,5	1,7	46,81

After performing confining triaxial tests, it was noticed that shear strength of the clay shales was strongly influenced by the heating temperature. As the temperature elevated, samples became much stronger, which is indicated by increasing cohesion values and friction angle. Cohesion is the force between grain particles, that keeps them together, whereas friction angle is the resistance between particles during shearing. When the temperature increases, absorbed water gets out of the pores bringing particles closer (thinning water films). As the consolidation is applied by confining pressures, interlocking between the particles becomes greater, increasing the inner friction resistance of grain particles.

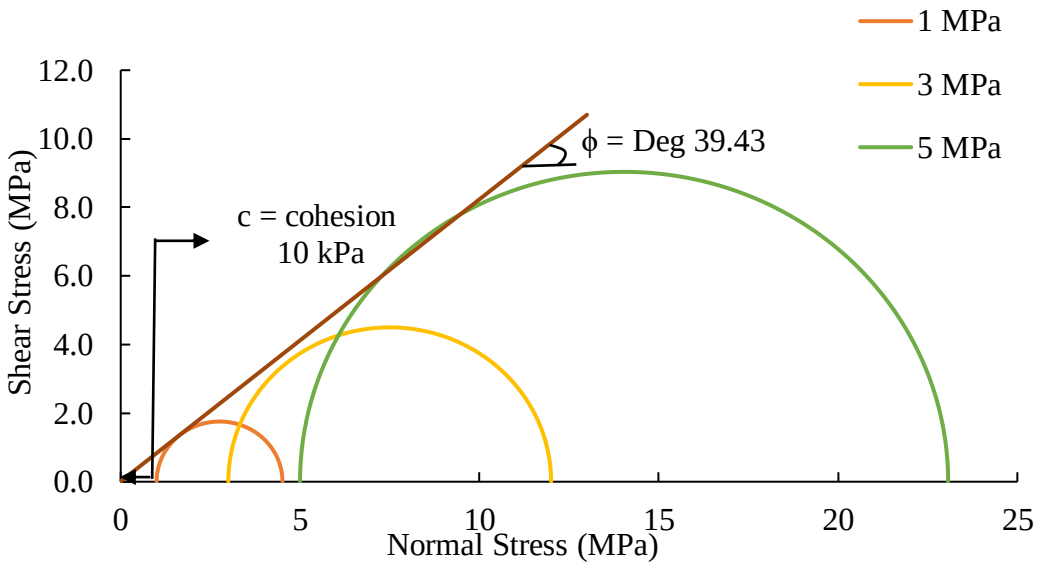

Figure 4.23: Mohr circles and failure envelope for three clay shale specimens thermally treated at 20°C under 1 MPa, 3 MPa and 5 MPa confining pressures

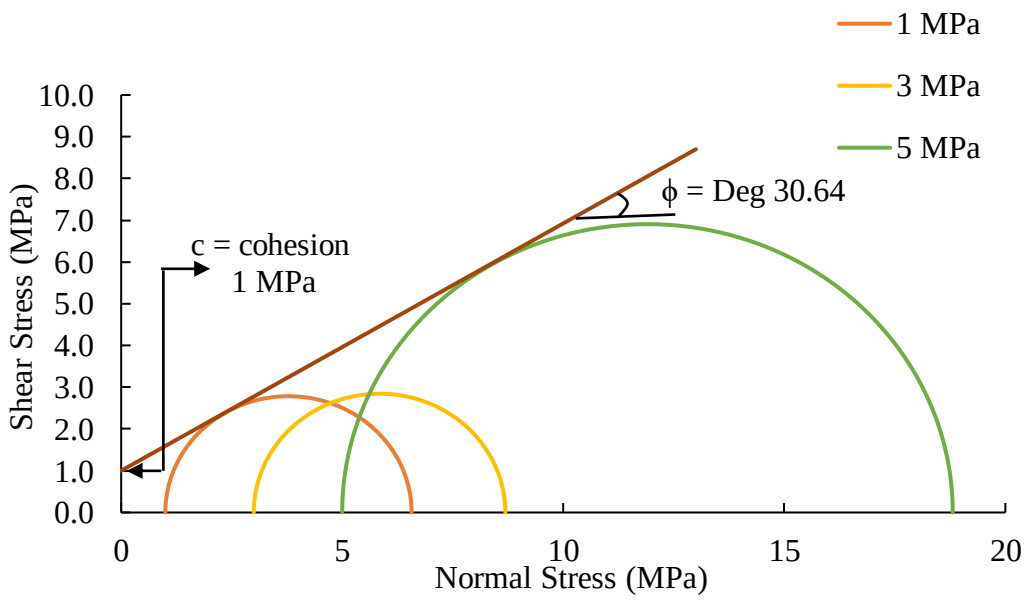

Figure 4.24: Mohr circles and failure envelope for three clay shale specimens thermally treated at 150°C under 1 MPa, 3 MPa and 5 MPa confining pressures

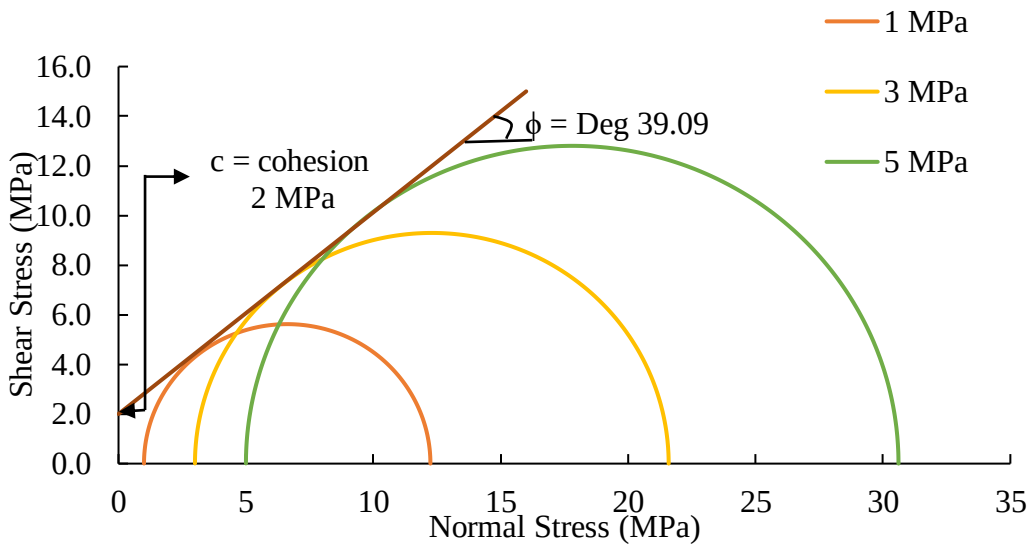

Figure 4.25: Mohr circles and failure envelope for three clay shale specimens thermally treated at 300°C under 1 MPa, 3 MPa and 5 MPa confining pressures

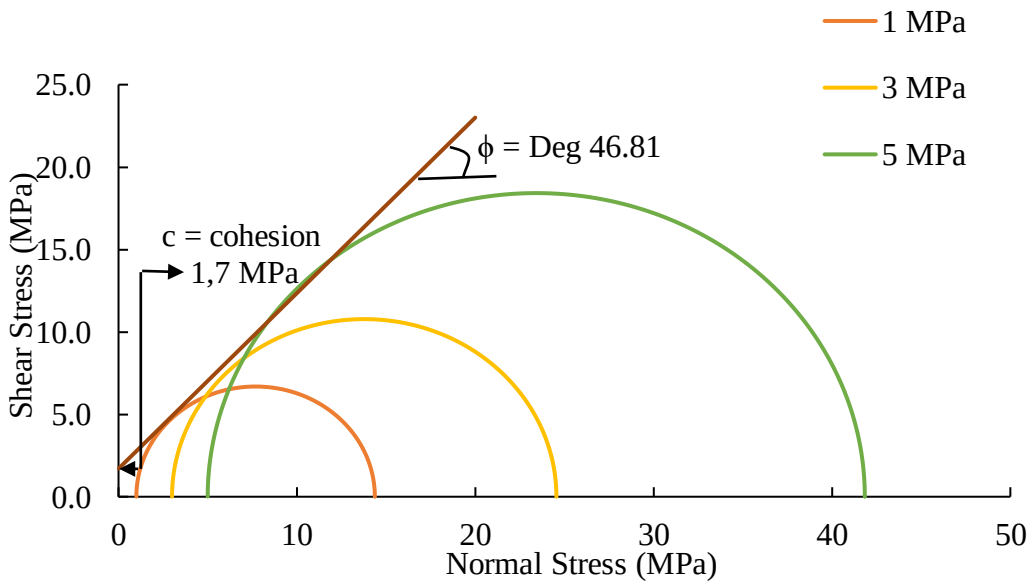

Figure 4.26: Mohr circles and failure envelope for three clay shale specimens thermally treated at 600°C under 1 MPa, 3 MPa and 5 MPa confining pressures

Further analysis was conducted to understand the effect of pre-heat treatment on friction angle. The below equation was governed to understand the sample disturbance by pre-heat treatment:

$$SD = \left(\frac{d_{i-s}}{d_f} - 1\right) * 100 \quad (3)$$

where SD is the disturbance of sample that was caused by pre-heat treatment (%), d_{i-s}, d_f are the in-situ and final densities of the sample obtained from the heating experiment, respectively. Obtained density and disturbance of sample values are presented in Table 4.4 and Figure 4.27. Results indicate that friction angle is related to the rate of sample disturbance. Less disturbed samples tend to have higher friction angle, whereas the samples that were disturbed the most by heating were have a lower friction angle, as shown in the figure.

Table 4.4: Disturbance of sample obtained using initial and final densities

T (°C)	Sample	Initial density	After heating	Disturbance of sample	
20	T20C1	1.89		8.70	10.00
	T20C3	1.87		9.66	10.95
	T20C5	1.88		9.18	10.48
150	T150C1	1.95	1.91	5.80	7.14
	T150C3	1.63	1.61	21.26	22.38
	T150C5	1.78	1.75	14.01	15.24
300	T150C1	1.99	1.73	3.86	5.24
	T150C3	1.95	1.72	5.80	7.14
	T150C5	1.93	1.69	6.76	8.10
600	T600C1	1.97	1.7	4.83	6.19
	T600C3	2.01	1.78	2.90	4.29
	T600C5	1.94	1.65	6.28	7.62

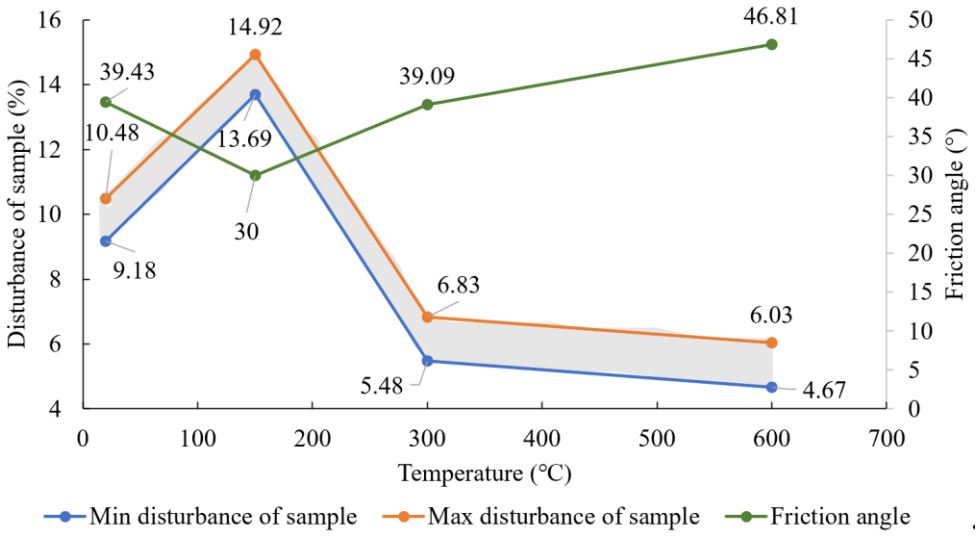

Figure 4.27: Friction angle and disturbance of sample versus temperature

4.3 Summary

The physical and mechanical behavior of clay shale is substantially affected by the variation of confining pressure and temperature. The colour changed from black to grey from ambient temperature 300℃ was associated with the organic matter combustion and surface and interlayer water evaporation. Above 300℃ the colour turned to yellowish brick-red due to the hematite formation. In addition, significant drop was observed in quartz above 300℃.

Chapter 5

5 Conclusions and recommendations for future work

5.1 Conclusions

Effects of thermal treatment on physical and mechanical properties of a clay shale from Wabiskaw member, near Long Lake site, Alberta, were investigated with triaxial compression tests at three different confining pressures (1, 3 and 5 MPa) and at pre-heated temperatures (20, 150, 300 and 600℃). The main conclusions from laboratory experiments can be drawn as follows:

Apparent changes in color are observed at a temperature of 150℃, turning from black to grey, which gradually became lighter at 400℃ and yellowish around 600℃. Additionally, the formation of cracks reached their peak within the temperature range of 300℃ and 400℃, from there on number of cracks and their shape slowly decreased with the increase in temperature.

A significant amount of reduction in weight and density occurred below 300℃. At that temperature, weight loss was found to be 15.5%, accounting for 89% of the total weight loss and the density loss was 19.6%. The continued increase in temperature did not result in any substantial changes in weight and density of a specimen.

The XRD results indicated significant reduction in intensity of quartz from 20℃ to 300℃ while showing little to no change after 300℃. This reduction is related to quartz being in a partially amorphous state and contributed to the stiffening of the sample. In addition, no major changes were recorded in clay mineralogy at a temperature range of 300℃ to 600℃ except slight increase in quartz. Moreover, XRF analysis at the same temperatures showed oxides contained in clay. Based on XRF analysis, the color change of the sample to initially darker colors are related to combustion of organic material. However, further color change to yellowish colors is due to formation of hematite (Fe_2O_3) as heating took place in oxidizing environment.

Deformation modulus shows increasing trends with the increment of treatment temperature and confining pressure. An increase in deformation modulus was related to the moisture content loss of the samples. In addition, deformation modulus increased at the low confining pressure while decreased at high confining pressure. Moreover, Poisson's ratio decreased with increasing temperature and confining pressure. This also confirmed that samples became more brittle with heat treatment.

Peak strength of clay shale is strongly and directly influenced by temperature. Distribution of peak strength values is somehow scattered and non-linear at lower treatment temperatures. However, after heating temperature of 300℃ and 600℃, peak strengths of specimens are 2 to 2.5 times greater in comparison with the ambient one. Similar increment in strength is observed when the confining pressure increased from 1 MPa to 5 MPa.

5.2 Recommendations for future work

The recommendations for future studies are:

1. Considering shale rocks anisotropy, bedding orientation might greatly affect the physical and mechanical behaviors at various heating temperatures and confining pressures. Therefore, the test to identify the effect of the fracture orientation would give more accurate results on factors affecting sample failure.
2. In triaxial compression tests, radial confining stresses applied in both directions were the same (inside a cell filled with fluid), which neglects the intermediate and minimum principal stresses by considering them equal. However, all three principal stresses could be different with unequal magnitudes under real conditions. Hence it is recommended to use true triaxial compression tests, which permit all three stresses to be regulated.
3. Clay mineralogy was obtained using XRD after treating at temperatures of 300℃, 400℃, 500℃ and 600℃. It is recommended to investigate the clay mineralogy at low temperatures with lower temperature intervals.

Appendix - Stress – strain curves

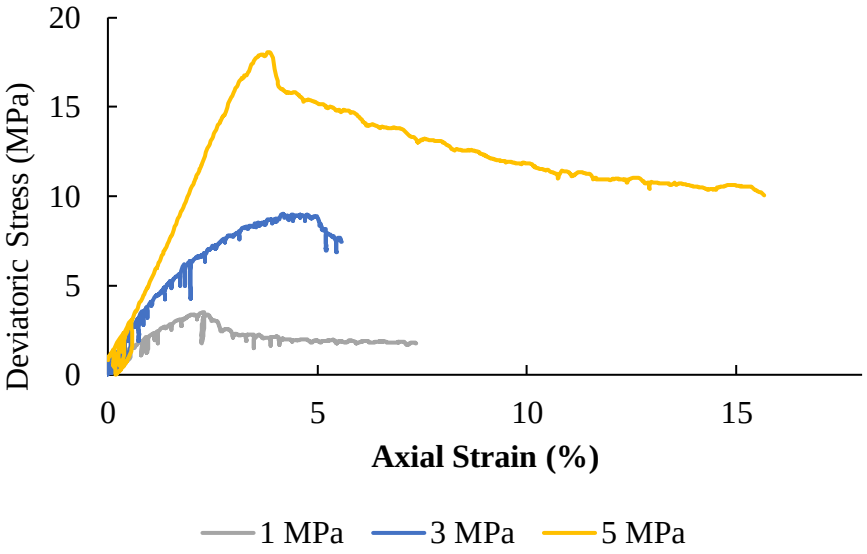

Figure A.0.1: Deviatoric stress vs axial strain at treatment temperature of 20℃ under confining pressures of 1 MPa, 3 MPa and 5 MPa

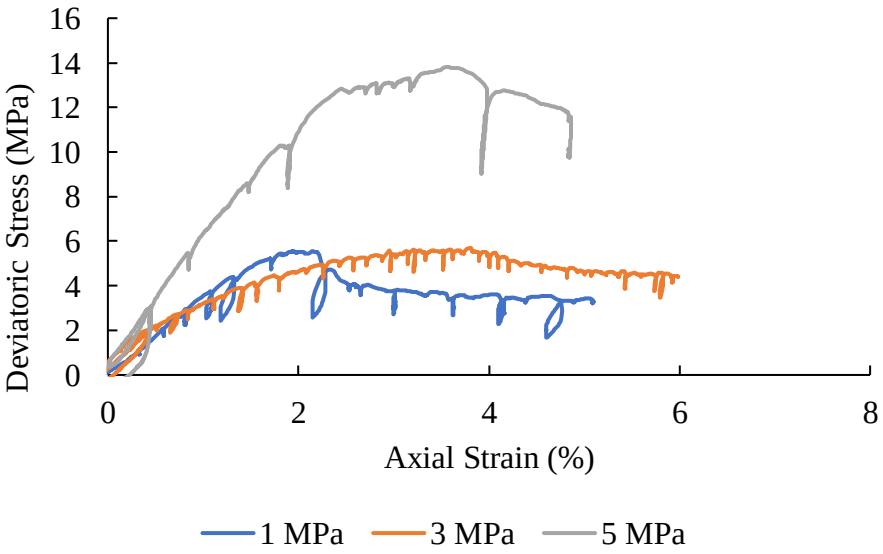

Figure A.0.2: Deviatoric stress vs axial strain at treatment temperature of 150℃ under confining pressures of 1 MPa, 3 MPa and 5 MPa

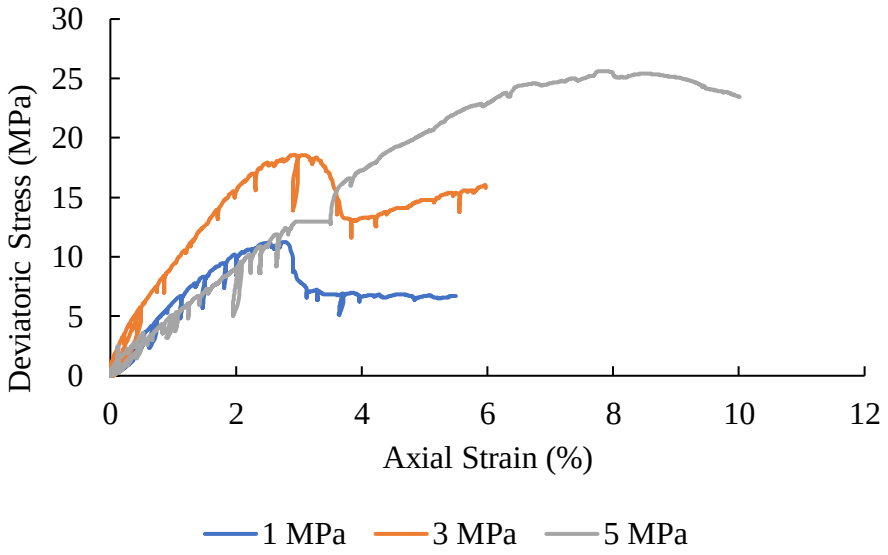

Figure A.0.3: Deviatoric stress vs axial strain at treatment temperature of 300℃ under confining pressures of 1 MPa, 3 MPa and 5 MPa

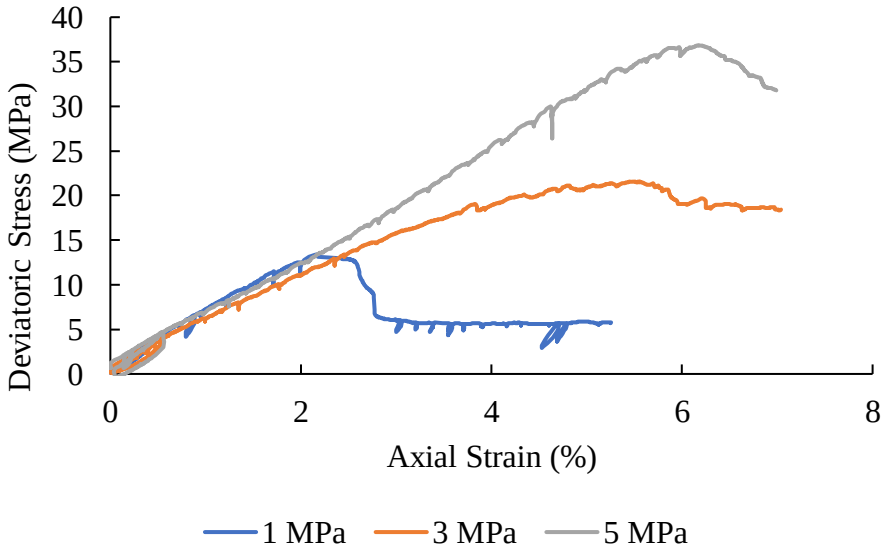

Figure A.0.4: Deviatoric stress vs axial strain at treatment temperature of 600℃ under confining pressures of 1 MPa, 3 MPa and 5 MPa

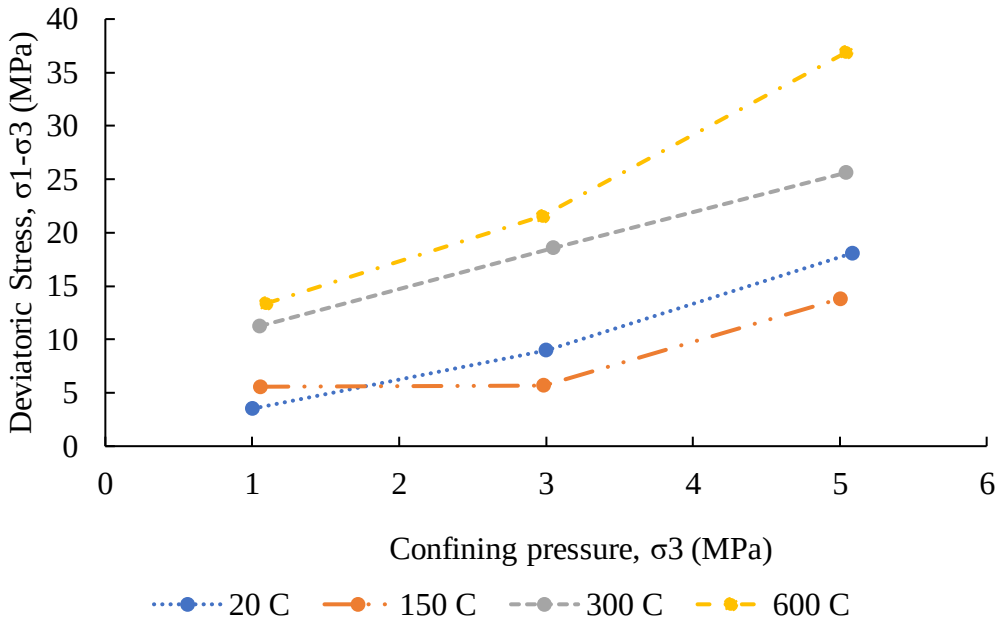

Figure A.0.5: Relationship between deviatoric stress vs confining pressure at different temperatures

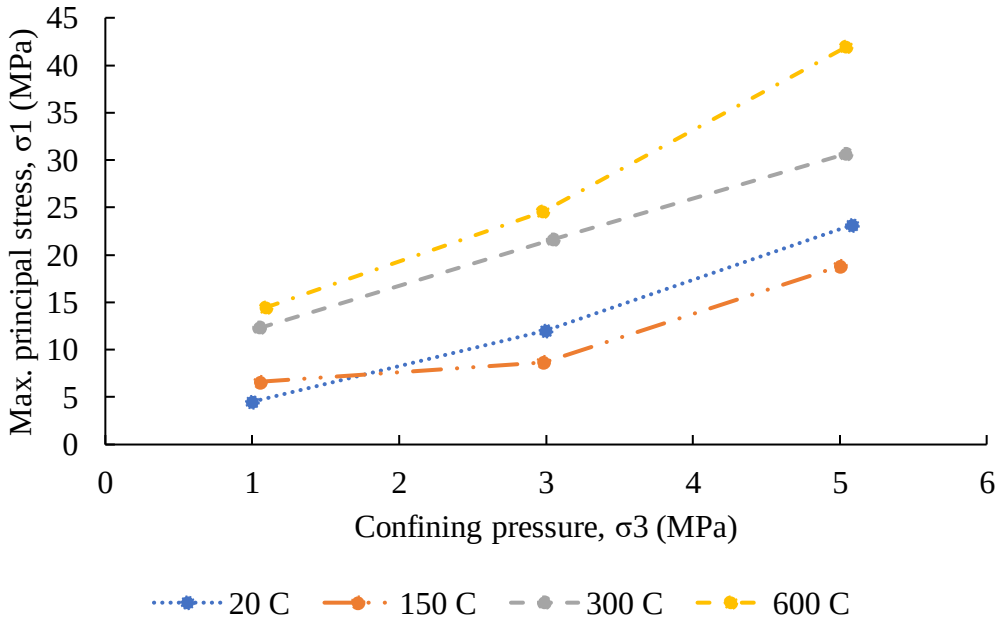

Figure A.0.6: Relationship between maximum principal stress vs confining pressure at different temperatures

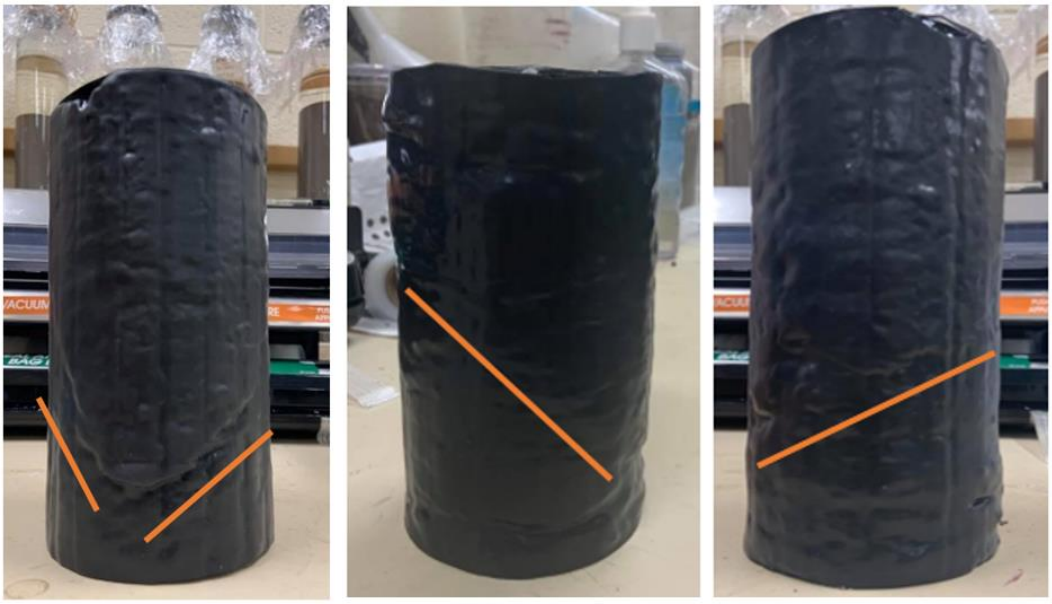

Figure A.7: Visual observation of shear failure on samples after experimentation

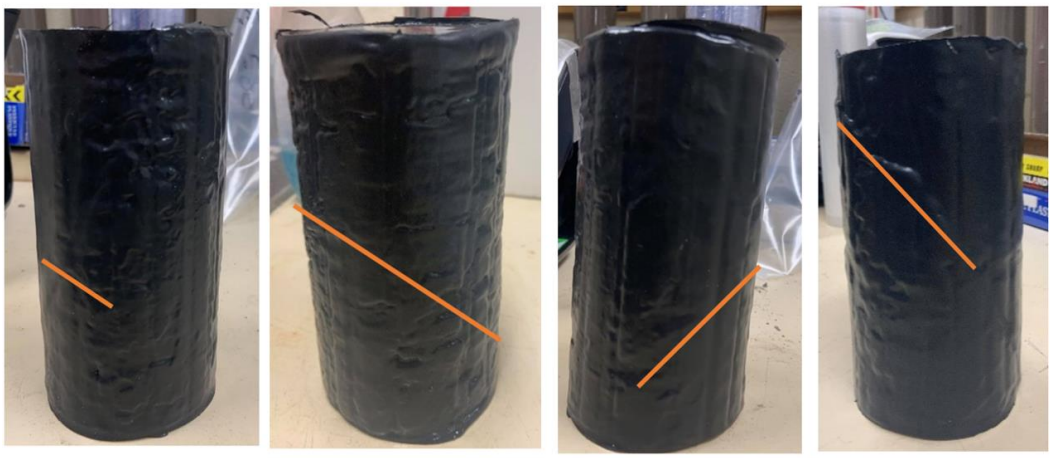

Figure A.8: Visual observation of shear failure on samples after experimentation

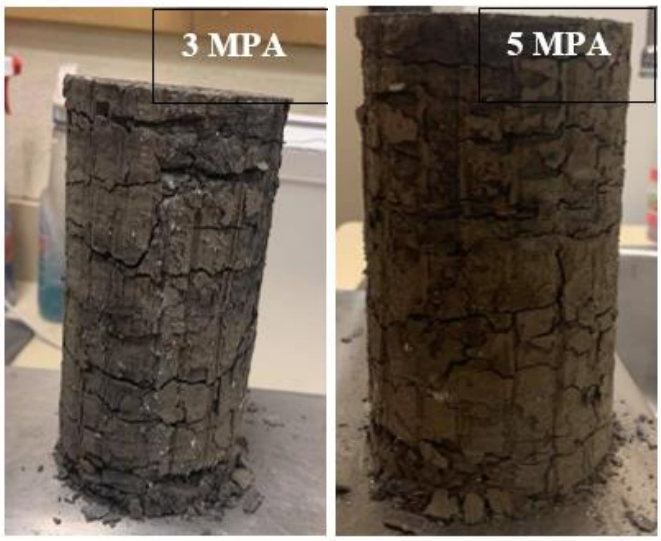

Figure A.9: Visual microstructure and macrostructure observation of the samples for experiments at 150℃. Results were influenced due to the cracking pattern

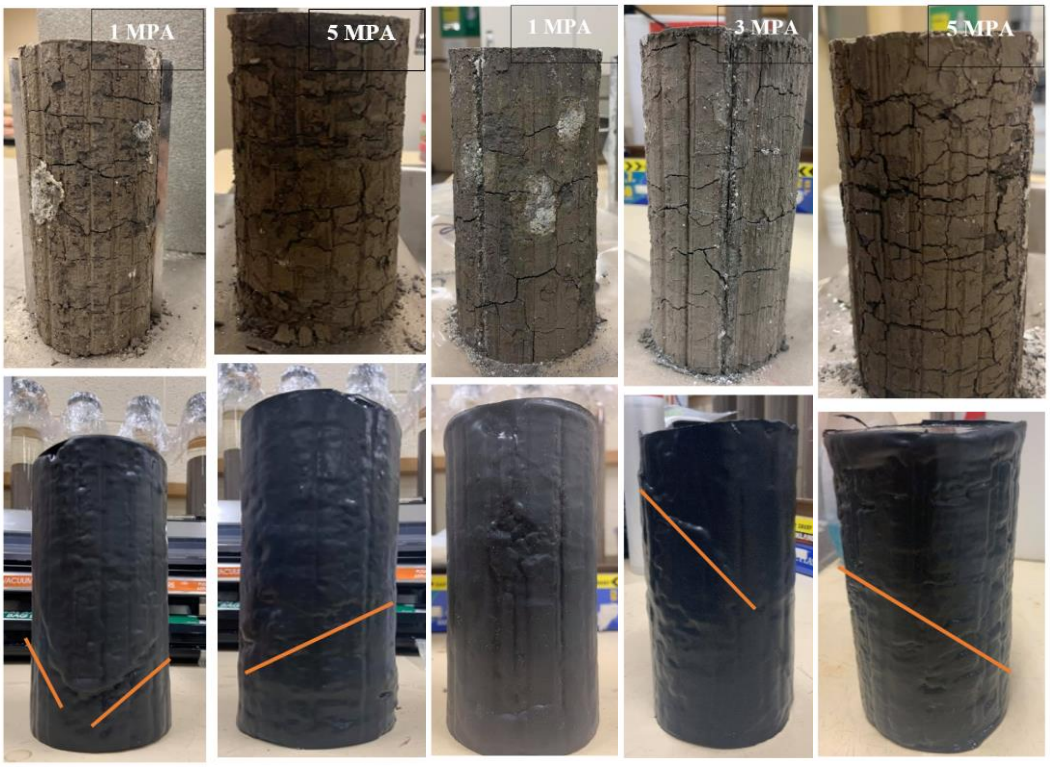

Figure A.10: Side view of samples obtained before and after experiments

References

Abed, A., & Korkiala-Tanttu, L. (2018). *Stability analysis for road-cutting: Review, recommendations and examples*. Liikenneviraston Tutkimuksia Ja Selvityksiä.

Aguilera, R. (2016). Shale gas reservoirs: Theoretical, practical and research issues. *Petroleum Research*, *1*(1), 10–26.

Amer, M., Alhesan, J., Marshall, M., Al-Ayed, O., & Awwad, A. (2019). Low temperature retorting of Jordanian oil shales using semi-continuous apparatus. *Journal of Analytical and Applied Pyrolysis*, *142*, 104639.

Amšiejus, J., Dirgėlienė, N., Norkus, A., & Žilionienė, D. (2009). Evaluation of soil shear strength parameters via triaxial testing by height versus diameter ratio of sample. *The Baltic Journal of Road and Bridge Engineering*, *4*(2), 54–60.

Banerjee, A., Puppala, A., Patil, U., Hoyos, L., & Bhaskar, P. (2018). *A simplified approach to determine the response of unsaturated soils using multistage triaxial test* (pp. 332–342).

Belyadi, H., Fathi, E., & Belyadi, F. (2019). Rock mechanical properties and in situ stresses. In *Hydraulic Fracturing in Unconventional Reservoirs* (pp. 215–231). Elsevier.

Boulin, P., Angulo-Jaramillo, R., Talandier, J., Berne, P., & Daian, J. (2012). Contribution of the dusty gas model to permeability/diffusion tests on partially saturated clay rocks. *Transport in Porous Media*, *93*(3), 609–634.

Carl, E., Liermann, H., Ehm, L., Danilewsky, A., & Kenkmann, T. (2018). Phase transitions of α-quartz at elevated temperatures under dynamic compression using

a membrane-driven diamond anvil cell: Clues to impact cratering? *Meteoritics & Planetary Science*, *53*(8), 1687–1695.

Castellanos, A., Ríos, R., Ramos, M., & Plaza, E. (2012). A comparative study of mineralogical transformations in fired clays from the Laboyos Valley, Upper Magdalena Basin (Colombia. *Boletín de Geología*, *34*(1), 43–55.

Chalaturnyk, R. J. (1996). *Geomechanics of the steam assisted gravity drainage process in heavy oil reservoirs*. University of Alberta Libraries. https://doi.org/10.7939/R39W0971Z

Chang, Y., Lu, H., Chen, B., Ji, Z., Wang, C., Qi, Y., Li, J., Du, X., & Yin, G. (2013). *Multi-fracture stimulation techniques make better wells in ultra-low permeability oil reservoirs*. SPE/AAPG/SEG Unconventional Resources Technology Conference.

Chen, Y., Wang, S., Ni, J., Azzam, R., & Fernandez, T. (2017). An experimental study of the mechanical properties of granite after high temperature exposure based on mineral characteristics. *Engineering Geology*, *220*, 234–242.

Cheng, M., Kotov, A., Pyke, K., & Hanif, A. (2015). Improvement in Heavy-Oil Reservoir Evaluation Using Nuclear Magnetic Resonance: Long Lake and Kinosis SAGD Projects, Alberta, Canada. *Petrophysics-The SPWLA Journal of Formation Evaluation and Reservoir Description*, *56*(03), 239–250.

Das, B. M., & Sivakugan, N. (2015). *Fundamentals of Geotechnical Engineering* (5th ed.). CENGAGE Learning Custom Publishing.

Devriese, S., & Oldenburg, D. (2016). Feasibility of electromagnetic methods to detect and image steam-assisted gravity drainage steam chambers. *Geophysics*, *81*(4), 227– 241.

Ding, Y., Wang, Y., Zhang, Y., & Paulini, P. (2009). Investigation of the stress and strain state of clay pipes under fire condition. *Ceramics International*, *35*(1), 63–67.

Dudley, B. (2018). *BP Energy Outlook* (9th ed.). Report–BP Energy Economics.

Elgamouz, A., Tijani, N., Shehadi, I., Hasan, K., & Kawam, M. (2019). Characterization of the firing behaviour of an illite-kaolinite clay mineral and its potential use as membrane support. *Heliyon*, *5*(8), 02281.

Favero, V., Ferrari, A., & Laloui, L. (2018). Anisotropic behaviour of opalinus clay through consolidated and drained triaxial testing in saturated conditions. *Rock Mechanics and Rock Engineering*, *51*(5), 1305–1319.

Florez, Horacio, & Gildin, E. (2019). Model-Order Reduction of coupled flow and geomechanics in Ultra-Low Permeability ULP reservoirs. *Day 2 Thu, April 11, 2019*.

Fontaine, F., Hatert, F., & Fagel, N. (2018). *High-temperature XRD investigations of phase transformation in mineralogy: Examples for clay used in ceramics and phosphate minerals*.

Gabova, A., Chekhonin, E., Popov, Y., Savelev, E., Romushkevich, R., Popov, E., & Kozlova, E. (2020). Experimental investigation of thermal expansion of organic-rich shales. *International Journal of Rock Mechanics and Mining Sciences*, *132*, 104398.

Geng, J., & Sun, Q. (2018). Effects of high temperature treatment on physical-thermal properties of clay. *Thermochimica Acta*, *666*, 148–155.

Golpour, H., & Smith, J. (2017). Oil Shale Ex-Situ Process-Leaching Study of Spent Shale. *International Journal of Engineering and Science Invention*, *6*, 45–53.

Grebowicz, J. (2014). Understanding thermal properties of oil shales at high temperature toward application of nuclear energy in extraction of natural hydrocarbons. *Journal of Thermal Analysis and Calorimetry*, *116*(3), 1481–1490.

Guo, Y., Huang, L., Li, X., Chen, J., & Sun, J. (2020). Experimental investigation on the effects of thermal treatment on the physical and mechanical properties of shale. *Journal of Natural Gas Science and Engineering*, *82*, 103496.

Hajpál, M. (2002). Changes in sandstones of historical monuments exposed to fire or high temperature. *Fire Technology*, *38*(4), 373–382.

Han, J., Sun, Q., Xing, H., Zhang, Y., & Sun, H. (2017). Experimental study on thermophysical properties of clay after high temperature. *Applied Thermal Engineering*, *111*, 847–854.

Hazra, B., Varma, A., Bandopadhyay, A., Chakravarty, S., Buragohain, J., Samad, S. K., & Prasad, A. K. (2016). FTIR, XRF, XRD and SEM characteristics of Permian shales, India. *Journal of Natural Gas Science and Engineering*, *32*, 239–255.

Hein, F. (2015). *The Cretaceous McMurray oil sands, Alberta, Canada: A world-class, tidally influenced fluvial–estuarine system—an Alberta government perspective* (Vol. 68, pp. 561–621). Elsevier.

Holditch, S. (2013). Unconventional oil and gas resource development–Let's do it right. *Journal of Unconventional Oil and Gas Resources*, *1*, 2–8.

Hongjun, W., Feng, M., Xiaoguang, T., Zuodong, L., Zhang, X., Zhenzhen, W., Denghua, L., Bo, W., Yinfu, X., & Liuyan, Y. (2016). Assessment of global unconventional oil and gas resources. *Petroleum Exploration and Development*, *43*(6), 925–940.

Hu, J., Yu, F., Lu, Y., Yan, Q., Wooten, J., Columbus, E. P., & Wei, L. (2011). Catalytic Conversion of Biomass-derived Syngas to Gasoline Range Hydrocarbons. In *2011 Louisville, Kentucky, August 7-10, 2011* (p. 1). American Society of Agricultural and Biological Engineers.

Huang, H., & Grasby, S. (2015). Recognition and sources of secondary biogenic gases in the oil sand areas, Western Canada Sedimentary Basin. *Bulletin of Canadian Petroleum Geology*, *63*(1), 20–32.

Húlan, T., Trnik, A., Štubňa, I., Bačík, P., Kaljuvee, T., & Vozar, L. (2015). Development of Young's modulus of illitic clay during heating up to 1100 C. *Materials Science (Medžiagotyra*, *21*, 429–434.

Hupp, B., & Donovan, J. (2018). Quantitative mineralogy for facies definition in the Marcellus Shale (Appalachian Basin, USA) using XRD-XRF integration. *Sedimentary Geology*, *371*, 16–31.

Jha, M. K., Verma, A., Gautam, P., & Negi, A. (2017). Study of mechanical properties of Vindhayan shaly rocks at elevated temperature. *Journal of the Geological Society of India*, *90*(3), 267–272.

Johnson, D., Hooper, P., & Conrey, R. (1999). XRF method XRF analysis of rocks and minerals for major and trace elements on a single low dilution Li-tetraborate fused bead. *Advances in X-Ray Analysis*, *41*, 843–867.

Kim, D., & Kim, J. (2007). Resilient behavior of compacted subgrade soils under the repeated triaxial test. *Construction and Building Materials*, *21*(7), 1470–1479.

Kosar, K. M. (1989). *Geotechnical properties of oil sands and related strata*. University of Alberta Libraries. https://doi.org/10.7939/R3959CK1F

Laloui, L., & Loria, A. (2019). *Analysis and design of energy geostructures: Theoretical essentials and practical application*. Academic Press.

Li, H., Lai, B., & Lin, S. (2016). Shale mechanical properties influence factors overview and experimental investigation on water content effects. *Journal of Sustainable Energy Engineering*, *3*(4), 275–298.

Liu, H., Cui, S., Meng, Y., Fan, Y., Liu, T., Yu, A., & Hu, Z. (2020). Wellbore stability evaluation method based on the continuous tangent envelope of a Mohr circle. *Science Progress*, *103*(1), 0036850419888465.

Masri, M., Sibai, M., & Shao, J. (2008). *Experimental study of the thermomechanical behavior of the petroleum reservoir*. SPE Eastern Regional/AAPG Eastern Section Joint Meeting.

Mazouz, E., Hamimed, M., Yahiaoui, A., Benzagouta, M., Khodja, M., Achi, N., & Duplay, J. (2020). Clay minerals in fluvial shaley sandstone of upper Triassic reservoir (TAGS)—Toual field SE Algeria: Identification from wireline logs and core data. *Arabian Journal of Geosciences*, *13*(9), 1–17.

Minaeian, V., Dewhurst, D., & Rasouli, V. (2017). Deformational behaviour of a clay-rich shale with variable water saturation under true triaxial stress conditions. *Geomechanics for Energy and the Environment*, *11*, 1–13.

Minardi, A., Giger, S. B., Ewy, R. T., Stankovic, R., Stenebråten, J., Soldal, M., Rosone, M., Ferrari, A., & Laloui, L. (2021). Benchmark study of undrained triaxial testing of Opalinus Clay shale: Results and implications for robust testing. *Geomechanics for Energy and the Environment*, *25*(100210), 100210.

Miras, A., Galán, E., González, I., RomeroBaena, A., & Martín, D. (2018). Mineralogical evolution of ceramic clays during heating. An ex/in situ X-ray diffraction method comparison study. *Applied Clay Science*, *161*, 176–183.

Mohajerani, M., Delage, P., Sulem, J., Monfared, M., Tang, A. M., & Gatmiri, B. (2014). The thermal volume changes of the Callovo–Oxfordian claystone. *Rock Mechanics and Rock Engineering*, *47*(1), 131–142.

Mohamadi, M., & Wan, R. (2016). Strength and post-peak response of Colorado shale at high pressure and temperature. *International Journal of Rock Mechanics and Mining Sciences*, *84*, 34–46.

Morodome, S., & Kawamura, K. (2009). Swelling behavior of Na-and Ca-montmorillonite up to 150 C by in situ X-ray diffraction experiments. *Clays and Clay Minerals*, *57*(2), 150–160.

Motghare, P., & Musale, A. (2017). Unconventional hydrocarbons: Gas hydrates-drilling challenges and suitable technology. *SPE Oil and Gas India Conference and Exhibition*.

Mumme, W., Tsambourakis, G., Madsen, I., & Hill, R. (1996). Improved petrological modal analyses from X-ray powder diffraction data by use of the Rietveld method; Part II, Selected sedimentary rocks. *Journal of Sedimentary Research*, *66*(1), 132–138.

Nasr, T., & Ayodele, O. (2005). Thermal techniques for the recovery of heavy oil and bitumen. *Proceedings of SPE International Improved Oil Recovery Conference in Asia Pacific*.

Nicksiar, M., & Martin, C. (2013). Crack initiation stress in low porosity crystalline and sedimentary rocks. *Engineering Geology*, *154*, 64–76.

Okada, T. (2005). *Mechanical properties of sedimentary soft rock at high temperatures* (pp. 1–4).

Oldakowski, K., Sawatzky, R., & Alvarez, J. (2016). *Geomechanical properties of clearwater shale at elevated temperatures*. SPE Canada Heavy Oil Technical Conference.

Ouahabi, M., Daoudi, L., Hatert, F., & Fagel, N. (2015). Modified mineral phases during clay ceramic firing. *Clays and Clay Minerals*, *63*(5), 404–413.

Patil, U. D., Puppala, A. J., Hoyos, L. R., & Pedarla, A. (2017). Modeling critical-state shear strength behavior of compacted silty sand via suction-controlled triaxial testing. *Engineering Geology*, *231*, 21–33.

Pugsley, T., Pernitsky, D., Grundler, J., & Johnsen, E. (2013). *Fouling of heat transfer surfaces in a steam assisted gravity drainage (SAGD) in situ facility for the recovery of oil sands bitumen*. 116–123.

Radovic, M., Lara-Curzio, E., & Riester, L. (2004). Comparison of different experimental techniques for determination of elastic properties of solids. *Materials Science & Engineering. A, Structural Materials: Properties, Microstructure and Processing*, *368*(1–2), 56–70.

Rahnema, H., Barrufet, M., & Mamora, D. (2017). Combustion assisted gravity drainage–Experimental and simulation results of a promising in-situ combustion technology to recover extra-heavy oil. *Journal of Petroleum Science and Engineering*, *154*, 513–520.

Rajeswari, A., Jackcina Stobel Christy, E., Gopi, S., Jayaraj, K., & Pius, A. (2020). Characterization studies of polymer-based composites related to functionalized filler-matrix interface. In *Interfaces in Particle and Fibre Reinforced Composites* (pp. 219–250). Elsevier.

Sagar, A., Oliver, H., & Chikkatur, A. (2005). Climate change, energy, and developing countries. *Vt. J. Envtl. L.*, *7*, 71.

Schock, R. N., Sims, R., Bull, S., Larsen, H., Likhachev, V., Nagano, K., Nilsson, H., Vuori, S., Yeager, K., Zhou, L., Zhang, X., & Weyant, J. (2012). Energy Supply Systems. In T. B. Johansson, N. Nakicenovic, A. Patwardhan, & L. Gomez-Echeverri (Eds.), *Global Energy Assessment (GEA)* (pp. 1131–1172). Cambridge University Press.

Shi, L., Xi, C., Liu, P., Li, X., & Yuan, Z. (2017). Infill wells assisted in-situ combustion following SAGD process in extra-heavy oil reservoirs. *Journal of Petroleum Science & Engineering*, *157*, 958–970.

Siegesmund, S., Ullemeyer, K., Weiss, T., & Tschegg, E. K. (2000). Physical weathering of marbles caused by anisotropic thermal expansion. *International Journal of Earth Sciences*, *89*(1), 170–182.

Środoń, J. (2006). Chapter 12.2 identification and quantitative analysis of clay minerals. In *Developments in Clay Science* (pp. 765–787). Elsevier.

Štubňa, I., Húlan, T., Kaljuvee, T., & Vozár, L. (2018). Investigation of dynamic mechanical properties of Estonian clay Arumetsa during firing. *Applied Clay Science*, *153*, 23–28.

Sun, Q., Zhang, W., & Qian, H. (2016). Effects of high temperature thermal treatment on the physical properties of clay. *Environmental Earth Sciences*, *75*(7). https://doi.org/10.1007/s12665-016-5402-2

Sygala, A., Bukowska, M., & Janoszek, T. (2013). High temperature versus geomechanical parameters of selected rocks–the present state of research. *Journal of Sustainable Mining*, *12*(4), 45–51.

Tian, H., Ziegler, M., & Kempka, T. (2014). Physical and mechanical behavior of claystone exposed to temperatures up to 1000 °C. *International Journal of Rock Mechanics and Mining Sciences (Oxford, England: 1997)*, *70*, 144–153.

Tian, Hong, Kempka, T., Xu, N.-X., & Ziegler, M. (2012). Physical properties of sandstones after high temperature treatment. *Rock Mechanics and Rock Engineering*, *45*(6), 1113–1117.

Trindade, M. J., Dias, M. I., Coroado, J., & Rocha, F. (2010). Firing tests on clay-rich raw materials from the Algarve basin (southern Portugal): Study of mineral transformations with temperature. *Clays and Clay Minerals*, *58*(2), 188–204.

Trník, A., Štubňa, I., Varga, G., Bačík, P., & Podoba, R. (2011). Young's modulus of heatproof tile ceramics Letovice during firing. *Journal of the Ceramic Society of Japan*, *119*(1392), 645–649.

Xia, T., Greaves, M., Turta, A., & Ayasse, C. (2003). THAI—A 'short-distance displacement'in situ combustion process for the recovery and upgrading of heavy oil. *Chemical Engineering Research and Design*, *81*(3), 295–304.

Yan, S., Zhuo, L., Jiang, Z., Qun, L., Dongdong, L., & Zhiye, G. (2017). Progress and development trend of unconventional oil and gas geological research. *Petroleum Exploration and Development*, *44*(4), 675–685.

Yu, Y., Liang, W., Bi, J., Geng, Y., Zhang, C., & Zhao, Y. (2015). *Thermophysical experiment and numerical simulation of thermal cracking and heat transfer for oil shale*.

Zhang, L., Mao, X., Liu, R., Li, Y., & Yin, H. (2014). Meso-structure and fracture mechanism of mudstone at high temperature. *International Journal of Mining Science and Technology*, *24*(4), 433–439.

Zhou, B. (2019). *Feasibility Study of Lean Oil Sand as Base and Surface Material on Gravel Roads in Alberta*. University of Waterloo.

Zou, C., Tao, S., Yang, Z., Yuan, X., Zhu, R., Hou, L., Jia, J., Wang, L., Wu, S., & Bai, B. (2012). New advance in unconventional petroleum exploration and research in China. *Bulletin of Mineralogy, Petrology and Geochemistry*, *31*(4), 312–322.

Zouaoui, H., & Bouaziz, J. (2017). Physical and mechanical properties improvement of a porous clay ceramic. *Applied Clay Science*, *150*, 131–137.